Wireless Power Transfer Systems Using Metamaterials: A Review

WOOSOL LEE, (Graduate Student Member, IEEE), AND **YONG-KYU YOON**, (Member, IEEE)
Department of Electrical and Computer Engineering, University of Florida, Gainesville, FL 32611, USA

Corresponding authors: Woosol Lee (leewoosol@ufl.edu) and Yong-Kyu Yoon (ykyoon@ece.ufl.edu)

ABSTRACT With the recent advancement and progress in the field of wireless power transfer (WPT), there is an ever increasing demand for high power transfer efficiency (PTE) of the WPT systems and improved transfer distance for the end-users. However, some existing WPT systems have limited PTE and transfer distance as they take the inductive coupling approach, where the PTE dramatically decreases as the distance between (Tx) and receiver (Rx) coils increases. Alternatively, magnetic resonance coupling (MRC) is used as a mid-range WPT approach, for which the insertion of metamaterials (MTMs) between Tx and Rx coils is exploited to improve efficiency. MTMs are artificially engineered materials that show uncommon electromagnetic properties, such as evanescent wave amplification and negative refractive characteristics, which could be utilized for the enhancement of PTE. In this article, a comprehensive review on recent progresses in the MTM-based WPT systems is reported, where previously reported MTM-based WPT systems are compared in terms of various parameters such as configurations, operating frequencies, dimensions and PTE. Also, the PTEs of these systems were plotted as a function of the normalized transfer distance. This review is expected to provide an insight for understanding the trends of the MTM-based WPT systems and serve as a reference for researchers who work on WPT systems and their applications.

INDEX TERMS Wireless power transfer (WPT), metamaterials (MTMs), power transfer efficiency (PTE), energy harvesting.

I. INTRODUCTION

Recently, the research and development on wireless power transfer (WPT) has been actively carried out in various areas. This energy transmission in a cordless way can change our traditional usage of the energy in diverse applications, such as implantable devices, mobile electronics, unmanned aerial vehicles (UAVs), electric vehicles (EVs), space satellites and so forth. Thanks to its properties of mobility, flexibility, location independency and ubiquity, the WPT technology has been an ideal solution for powering electronic devices.

WPT, which denotes transmitting electromagnetic energy from a power source to a load without conductor connection, is not a new concept. In the past decades, several researchers have observed the transmission of electrical energy without wires, however the absence of a logical theory attributed these phenomena ambiguously to electromagnetic induction.

The associate editor coordinating the review of this manuscript and approving it for publication was Davide Ramaccia.

The beginning of the concise explanation of WPT dates back to the 1860s, when James Clerk Maxwell demonstrated Maxwell's equations, establishing a theory that combined electricity and magnetism to electromagnetism, predicting the existence of electromagnetic waves as the wireless carrier of electromagnetic energy. In addition, other mathematical models, and experiments for WPT have been investigated. In 1891, the first remarkable development in WPT technology was demonstrated by Tesla [1]. Tesla experimented with transmitting power by inductive and capacitive coupling using spark-excited radio frequency (RF) resonant transformers, now called Tesla coils, which generated high alternating current (AC) voltages. In his wireless light bulb experiments, he figured out he could increase the distance by using a receiving LC circuit tuned to resonance with the transmitter's LC circuit, using resonant inductive coupling. On the other hand, Brown [2] first exhibited a microwave power transfer system realizing long-distance wireless energy transfer at Raytheon in 1963. In recent years, the non-radiative WPT systems which are inductive and magnetic resonant coupling

WPT have become more pervasive in mobile consumer electronics.

WPT technology can be divided into two categories, namely, near-field and far-field WPT. Near-field refers to a WPT system with a transfer distance less than its operating wavelength. The most widely used technologies corresponding to this classification are inductive coupling based WPT and magnetic resonant coupling (MRC)-based WPT. However, even though the MRC-based WPT can extend the power transfer to a mid-range distance (cm $\sim$ m), the increase of the transfer distance reduces the magnetic coupling between the transmitter (Tx) and receiver (Rx) coils so that the power transfer efficiency (PTE) of the system degrades, and the transfer distance of the MRC-based WPT system is limited [3]. As for the far-field WPT, microwave energy transfer called radiative WPT belongs to this category. In the radiative WPT mechanism, radiative power emitted from a transmitter antenna propagates through the air over a far distance. This electromagnetic (EM) wave can be captured by a rectenna (rectifier and antenna) and rectified to DC power. But, as radio waves propagate into the air in omni-direction, losses occur during far distance propagation, thereby making PTE comparable low. Moreover, there are design challenges for a rectenna, such as difficulty in the feeding network design to realize effective beamforming for high PTE, mutual coupling between antenna elements degrading rectenna performance, and high loss of array feeding network, and so forth.

In recent years, researchers have reported that metamaterials (MTMs) can be utilized for improving the transfer efficiency of the near-field WPT system, called MTM-based WPT system, and taking advantage of adopting the far-field WPT system design. MTMs are artificially engineered materials that show uncommon and exotic electromagnetic properties, such as evanescent wave amplification and negative refractive characteristics, and so on [4]. These non-traditional phenomena provide innovative mechanisms for WPT and RF energy harvesting. More and More studies have been conducted in order to take advantage of metamaterials in the field of WPT and RF energy harvesting. However, it should be noted that still only a few reviews about MTMs in the WPT field have been reported [5]–[7]. Even though they summarized the previous works, they did not provide a comprehensive overview in terms of the performances and relevant design parameters of the WPT systems which should be critical for understanding the trends in the WPT technologies. Therefore, this review paper covers fundamentals of MTMs, previous advancements in MTMs for near-field WPT systems and their comparison, the perspectives, and future opportunities of MTM-based WPT systems.

The rest of this article is organized as followings. Section II introduces fundamentals of MTMs and their classification. The previously reported studies on MTM-based WPT technologies in the near-field will be summarized and discussed in Section III. In Section IV, the perspectives, future opportunities, and directions of MTMs in the WPT applications
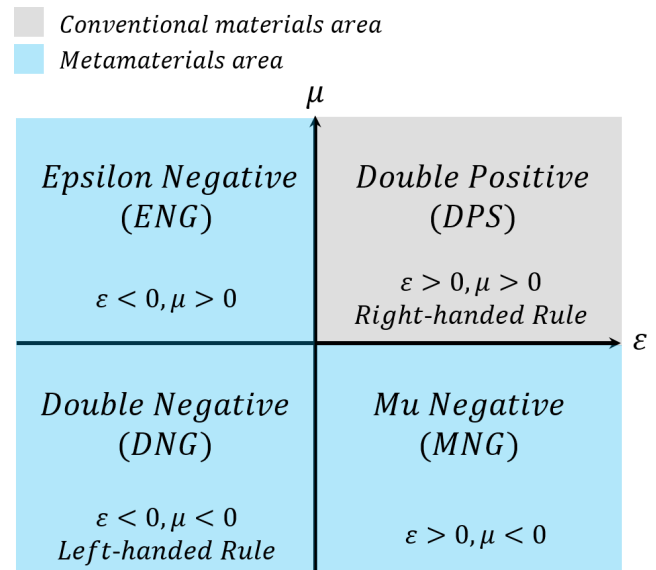

FIGURE 1. The categorization of materials based on permeability (μ) and permittivity (ε) values.

will be discussed. Lastly, the conclusion will be remarked in Section V.

II. FUNDAMENTAL OF METAMATERIALS

The prefix "meta" in metamaterials is from the Greek word $\mu\varepsilon\tau$ (meta), meaning "beyond". Following this origin, MTMs are defined as artificial engineered materials exhibiting uncommon and exotic properties that cannot be readily found in naturally occurring materials, thus, going beyond the limitations encountered when using traditional materials in the microwave and optical applications [4], [8]. The first theoretical investigation of MTMs was reported by Veselago in 1968 who introduced the electrodynamics of substances with the simultaneously negative values of electric permittivity and magnetic permeability which are the properties of MTMs [9].

As the permittivity and permeability are two parameters representing the electromagnetic properties of materials, materials can be categorized by four regions according to the polarities of permittivity and permeability [10]. As shown in Fig. 1, when the polarities of permittivity and permeability are positive simultaneously, the materials are classified as double-positive (DPS) materials which are the conventional materials. If the materials have the values of negative permittivity and positive permeability ($\varepsilon < 0, \mu > 0$), these are categorized as epsilon-negative (ENG) materials. When the permittivity is positive and permeability is negative ($\varepsilon > 0, \mu < 0$), these materials called mu-negative (MNG) materials. Especially, when it is configured to have these two parameters be both negative, these are defined as double-negative (DNG) materials and in general are known as MTMs. In addition, ENG and MNG materials also can be classified as the MTMs when they show such uncommon

properties at frequencies where conventional materials do not show.

When the values of both permittivity and permeability are simultaneously positive or negative, an electromagnetic wave can pass through the media. In the conventional materials (DPS) media, the electric, magnetic, and wave vectors follow the right-handed rule while the Poynting vector is parallel to the wave vector which means the energy decays along with propagation. On the other hand, as for the MTMs (DNG) media, the electric, magnetic, and wave vectors correspond to the left-handed rule and the Poynting vector has the opposite direction of wave propagation, hence, the energy flow is anti-parallel to the phase propagation direction of the source [11]. For this reason, the MTMs are also called left-handed materials [12], [13] or backward-wave media [14].

Moreover, the negative permittivity and permeability values of the DNG materials lead to the negative refractive index of the electromagnetic wave propagating through the media. The refractive index is an electromagnetic phenomenon that occurs between two materials. The DPS and DNG materials follow Snell's law, which states the relationship between the incident angle and the resulting refracted angle of EM wave transmission at the interface of two materials as Eq. (1).

$$n_1 sin\theta_1 = n_2 sin\theta_2 \quad (1)$$

where n_1, n_2, θ_1, and θ_2 are the refractive index of material 1 and 2, incident and refractive angles, respectively. From the materials perspective, the behavior of the refractive index is described using the permittivity and permeability, $n = \pm\sqrt{\varepsilon\mu}$ [15]. As for the MTMs, the refractive index can be described as $n = -\sqrt{\varepsilon\mu}$, because of the DNG property. It means the incident wave and the refractive wave are on the same side from the orthogonal line of the interface of the two media. Fig. 2 graphically shows the aforementioned different propagation paths with respect to the DPS and DNG media, respectively.
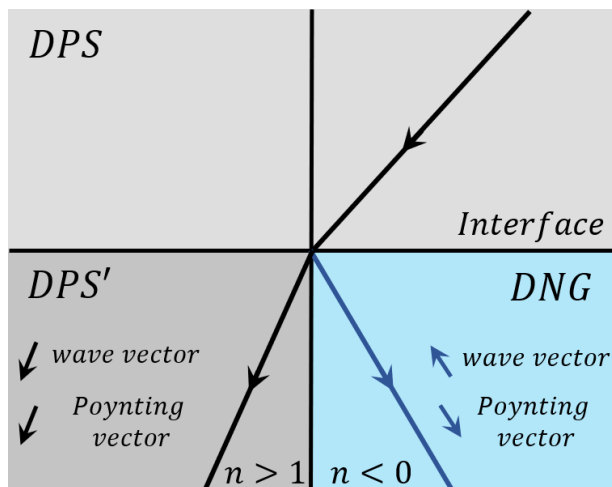

FIGURE 2. Refraction in the DPS (conventional) media and DNG (metamaterial) media.

In addition to the negative refraction property, an evanescent wave amplification is one of the important properties of MTMs. The proof of the evanescent wave amplification property was reported by Pendry [16] in 2000. By assuming S-polarized light propagating in vacuum, the electric field is given by

$$\mathbf{E}_{0S+} = [0, 1, 0] \exp(ik_z z + ik_x x - i\omega t) \quad (2)$$

where the axis of the lens to be the z-axis and the wave vector,

$$k_z = +i\sqrt{k_x^2 + k_y^2 - \omega^2 c^{-2}}, \quad \omega^2 c^{-2} < k_x^2 + k_y^2 \quad (3)$$

indicates exponential decay. At the interface with the MTM medium, some of light is reflected,

$$\mathbf{E}_{0S-} = r [0, 1, 0] \exp(-ik_z z + ik_x x - i\omega t) \quad (4)$$

And some of light transmitted into the MTM medium,

$$\mathbf{E}_{1S+} = m [0, 1, 0] \exp(ik'_z z + ik_x x - i\omega t) \quad (5)$$

where

$$k'_z = +i\sqrt{k_x^2 + k_y^2 - \varepsilon\mu\omega^2 c^{-2}}, \quad \varepsilon\mu\omega^2 c^{-2} < k_x^2 + k_y^2 \quad (6)$$

Casualty demands that we select this form of the wave in the MTM medium: it must decay away exponentially from the interface. By matching wave fields at the interface,

$$m = \frac{2\mu k_z}{\mu k_z + k'_z}, \quad r = \frac{\mu k_z - k'_z}{\mu k_z + k'_z} \quad (7)$$

Contrarily, a wave inside the MTM medium incident on the interface with vacuum realizes transmission and reflection as follows:

$$m' = \frac{2k'_z}{k'_z + \mu k_z}, \quad r' = \frac{k'_z - \mu k_z}{k'_z + \mu k_z} \quad (8)$$

Sum of multiple scattering events for calculating transmission through both surfaces of the MTM medium is

$$T_S = mm'\exp(ik'_z d) + mm'r'^2\exp(3ik'_z d) + mm'r'^4 \exp(5ik'_z d) + \ldots = \frac{mm'\exp(ik'_z d)}{1 - r'^2\exp(2ik'_z d)} \quad (9)$$

where d is the thickness of the MTM medium. By plugging (8) into (9) and taking limit assuming $\varepsilon = -1$, $\mu = -1$,

$$\lim_{\varepsilon,\mu=-1} T_S = \lim_{\varepsilon,\mu=-1} \frac{mm'\exp(ik'_z d)}{1 - r'^2\exp(2ik'_z d)}$$

$$= \lim_{\varepsilon,\mu=-1} \frac{2\mu k_z}{\mu k_z + k'_z}$$

$$\times \frac{2k'_z}{k'_z + \mu k_z} \frac{\exp(ik'_z d)}{1 - \left(\frac{k'_z - \mu k_z}{k'_z + \mu k_z}\right)^2 \exp(2ik'_z d)}$$

$$= \exp(-ik'_z d) = \exp(-ik_z d) \quad (10)$$

The reflection coefficient is given by

$$\lim_{\varepsilon,\mu=-1} R_S = r + \frac{mm'r'\exp(2ik'_z d)}{1 - r'^2\exp(2ik'_z d)} = 0 \quad (11)$$

P-polarized evanescent waves also can be derived as follows:

$$
\begin{aligned}
\lim_{\varepsilon,\mu=-1} T_P &= \lim_{\varepsilon,\mu=-1} \frac{2\varepsilon k_z}{\varepsilon k_z + k_z'} \frac{2k_z'}{k_z' + \varepsilon k_z} \\
&\quad \times \frac{\exp(ik_z'd)}{1 - \left(\frac{k_z' - \varepsilon k_z}{k_z' + \varepsilon k_z}\right)^2 \exp\left(2ik_z'd\right)} \\
&= \exp\left(-ik_zd\right)
\end{aligned}
\tag{12}
$$

Therefore, the MTM medium can amplify evanescent waves [16]. In addition, MTMs have other unique characteristics, including the inversion of Vavilove-Cerenkov radiation, Goos-Hanchen shift, and reversed Doppler shift [12], [17]. By the virtue of their exotic properties, MTMs have been actively researched with great potential in the area of superlens, meta-lens antenna, invisible cloak, and so forth [18], [19].

Recently, researchers have reported that MTMs can be utilized for improving the transfer efficiency of the near-field and far-field WPT systems. In the area of near-field WPT system, when the MTM slab is placed between the Tx and Rx coils, the magnetic field lines can be focused due to the negative refraction property of MTM slab [20] and coupling between Tx and Rx coils can be enhanced due to the evanescent wave amplification property of MTM slab since the coupling of the WPT system is essentially coupling of evanescent waves [21]. Consequently, this behavior leads to the improvement of the transfer efficiency of the WPT system. For the near-field WPT system, the negative refractive property of MTMs can be realized by the negative relative permeability of MTMs. In general, the negative refractive property requires both relative permittivity and permeability to be negative. But, in the deep subwavelength limit, the magnetic field and electric field decouple, and only one parameter is needed to achieve a negative refractive property. In most near-field resonant WPT systems, they fall in the deep subwavelength limit, since the size of the system is much smaller than the wavelength of the wave at the frequency of interest. For this reason, the negative relative permeability of the MTMs can be directly translated to the negative refractive index in the near-field WPT system. In general, these negative permeability MTMs for the near-field WPT systems are formed using periodic arrays of LC resonators (unit cells). The MTM unit cells are very close to one another so that a current circulating one cell produces a significant magnetic flux through the neighboring cells, thus, they are coupled through mutual inductance. If a resonant current is induced in one cell and the mutual inductance causes a current being inspired in the unit cells neighbors. These in turn inspire their neighbors resulting in the propagation of magneto-inductive waves (MIW) [22]. Based on the simplifying assumption that only the nearest neighbor interaction of the MTM unit cells is significant to MIW propagation, the dispersion equation of a 2-D array of MTM resonators is given by [22]

$$
\frac{\omega_0}{\omega} = \left(1 + k_x \cos\left(\gamma_x a\right) + k_y \cos\left(\gamma_y a\right)\right)^{-\frac{1}{2}}
\tag{13}
$$

where a is the periodicity of the array; k_x and k_y are coupling coefficients of the MTM unit cells in the horizontal and vertical direction, respectively; γ_x and γ_y are the complex propagation constants of MIWs. For $|\gamma_x a|$, $|\gamma_y a| \ll 1$, they describe propagating MIWs. The essential role of the MIWs in WPT systems is that the incident evanescent waves coming from the Tx coil strongly couple to the fields generated by MIW at the MTM interface and take energy from them, amplifying the evanescent waves [11], thereby enhancing the PTE of the WPT systems. Meantime, the MTMs also can be utilized in the far-field WPT system. By utilizing various structures of the MTMs, the rectenna can achieve the design flexibility, thereby taking diverse properties (e.g., small electrical size, multi-band, broadband, high gain) according to applications. In this article, further studies on the previously reported MTM-based WPT systems in near-fields will be summarized and discussed.

III. METAMATERIALS FOR THE NEAR-FIELD WPT SYSTEMS

As aforementioned, the near-field WPT systems have gained tremendous attention because of their applicability in diverse fields. However, most of the current WPT systems have restrictions in power transfer efficiency and distance as they use the inductive coupling approach. Meantime, the magnetic resonance coupling (MRC)-based WPT can be an alternative. The MRC-based WPT system can be realized when the Tx and Rx coils are designed to resonate at the same frequency [1]. Earlier, a two coil system has been investigated [23]. However, the increase of the transfer distance quickly degrades the transfer efficiency of the two-coil system, also the transfer efficiency is greatly influenced by load changes, and the practical transfer distance of the two-coil WPT system is limited. To improve the transfer efficiency and distance, various other approaches have been investigated such as a three-coil system [24], four-coil system [25], adaptive technique [26]–[28], frequency adaptive matching technique [29], coupling optimization approach [30], [28], and multi-resonator relay approach [31].

Alternatively, the usage of the MTM slab in the MRC-based WPT system had been investigated by Wang *et al.* [32], [33] a few years ago, which effectively improved the transfer efficiency of the WPT. After that, research on the MTM slab included MRC-based near-field WPT system has been actively studied in various ways. The common way to employ the MTM slab is to introduce one or more slabs between the Tx and the Rx coils to help focus the magnetic field toward the receiver coil and thus significantly improve PTE. In addition to this common architecture, various other architectures have been reported. As shown in Fig. 3, previously reported MTM-based near-field WPT architectures can be classified in terms of the dimension and position of the MTM slab. As for the dimension of the MTM slab, previous studies have mainly focused on one-dimensional (1-D), 2-D, and 3-D slabs which are composed of multiple MTM unit cells. On the other hand, MTM slabs have been
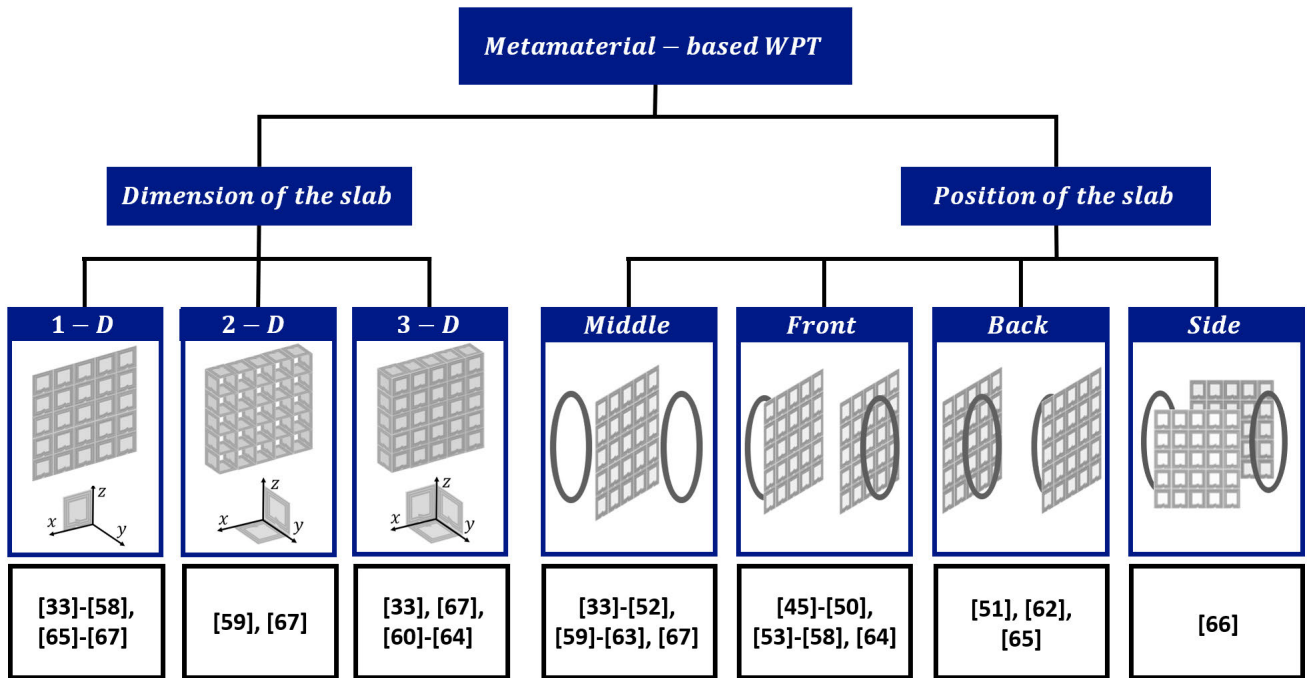
FIGURE 3. Classification of the previously reported metamaterial-based WPT.

used in different relative positions against the transmitting and receiving coils, such as the middle, front, back, and side of the WPT systems. In this section, more details on MTM-based WPT systems in near-field range will be discussed. Especially, some highlights on the previously reported works, and the performance comparison are provided.

FIGURE 4. Equivalent circuit of two-coil MRC-based WPT system.

A. METAMATERIAL-BASED WPT FOR A HIGH POWER TRANSFER EFFICIENCY

Transfer efficiency is one of the most important factors in WPT systems as the PTE of the WPT systems affects the transfer distance as well as the output power of the systems. In the MRC-based WPT systems, the PTE can be derived as follows [68]. In this section the PTE of two-coil WPT system (Fig. 4) is derived for the simplicity:

$$\eta = \frac{P_S}{P_L} = \frac{4 \cdot \frac{\omega^2 \cdot M^2 \cdot R_s \cdot R_L}{R_s^2 \cdot R_2^2}}{\left(\left(1 + \frac{R_s}{R_1}\right)\left(1 + \frac{R_L}{R_2}\right) + \frac{\omega^2 \cdot M^2}{R_1 \cdot R_2} \right)^2} \quad (14)$$

where η is the PTE; P_S and P_L are the source power and load power, respectively; ω is the operating frequency; M is the mutual inductance, where $M = k\sqrt{L_1 \cdot L_2}$; R_S, R_1, R_2 and R_L are the resistances of the source, resonator 1, 2, and load, respectively. In Eq. (14), the PTE is maximized when Eq. (15) is satisfied and the optimized PTE is given by equation (16) [68].
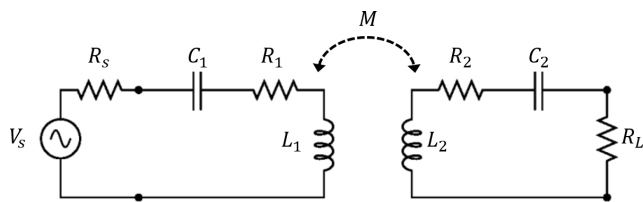
$$\frac{R_s}{R_1} = \frac{R_L}{R_2} = \sqrt{1 + \frac{\omega^2 \cdot M^2}{R_1 \cdot R_2}} \quad (15)$$

$$\eta_{opt} = \frac{k^2 Q_1 Q_2}{\left(1 + \sqrt{1 + k^2 Q_1 Q_2}\right)^2} = \frac{U^2}{\left(1 + \sqrt{1 + U^2}\right)^2} \quad (16)$$

where k is a coupling coefficient; Q_1 and Q_2 are the quality factors of resonator 1 and 2, respectively; U is a figure-of-merit for a WPT system where $U = k\sqrt{Q_1 \cdot Q_2}$. The MRC-based WPT systems where $U \gg 1$ are said to be strongly coupled, and ones where $U \ll 1$ are said to be weakly coupled [68]. It should be noted that the efficient WPT system can be achieved with high U which requires high k and high $Q's$ [68], [69]. Keeping this in mind, the properties of metamaterials (negative refraction and evanescent wave amplification) are of interest to MRC-based WPT systems since the MRC is essentially coupling of evanescent waves [32], [33]. In the status of resonance, electromagnetic (EM) fields are mostly focused inside the resonators. Outside the resonators, EM fields diminish evanescently and do not transfer energy. With the negative refraction index MTM slab, the amplitude of evanescent waves can be enhanced and the coupling coefficient of two resonators can be improved [32],

[33]. Finally, the improved coupling coefficient induces high U, thereby improving the PTE of the WPT systems by Eq. (16).
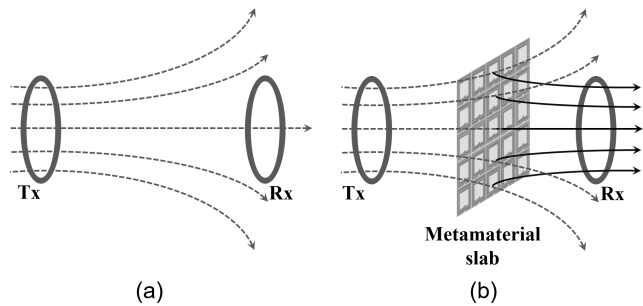

FIGURE 5. Conceptual principle of the metamaterial-based WPT: (a) WPT system without metamaterial slab, (b) with metamaterial slab (right).

By utilizing the aforementioned principle, MTM slabs are included to the WPT systems in various ways to get high PTE as depicted in Fig 3. They have utilized the unique properties of the MTMs which are negative refraction and evanescent wave amplification. Fig. 5 shows a conceptual schematic for the principle of the MTM-based WPT. In a WPT system (Fig. 5. (a)), the magnetic field generated by a Tx coil shows its flux lines symmetrically around the coil. If the Rx coil is located where the flux lines of the Tx coil reach, the cross-linked magnetic flux within the Rx coil will induce current flows in the Rx coil by Faraday's law, transferring power wirelessly. An issue is that not all the magnetic flux produced by the Tx coil is captured by the Rx coil, leaking out and leading to low PTE. Meantime, when a MTM slab is inserted between Tx and Rx as shown in Fig. 5. (b), the negative refraction index of the MTM slab will be able to focus the magnetic field lines effectively toward the Rx, thereby improving power transfer efficiency. Using this principle of the MTM-based WPT MTMs, various architectures with the different dimensions and different locations of MTM slabs have been studied.

Recently, Cho *et al.* [56] have reported the hybrid metamaterial slab (HMS), an attempt to optimize the topology of the multiple MTM unit cells. The proposed HMS consists of two different MTM unit cells to reduce the electromagnetic field (EMF) leakage in the WPT system, ultimately enhancing the PTE. In Fig. 6. (a), the focused magnetic field distribution of the WPT system with the HMS is depicted. The outer part of the HMS changes the diverging magnetic fields to the converging magnetic field due to the negative permeability of the type 1 unit cells and the center part of the HMS straightens the magnetic field due to the zero effective permeability of the type 2 unit cells. The structure and refraction property of the unit cells are shown in Fig. 6. (b) [56], where with the spiral type structure of the MTM unit cells, zero or negative permeability could be realized. It is shown that the value of the relative magnetic permeability changes the direction of the magnetic field to negative or zero by boundary conditions, for which experimental results have been performed with a
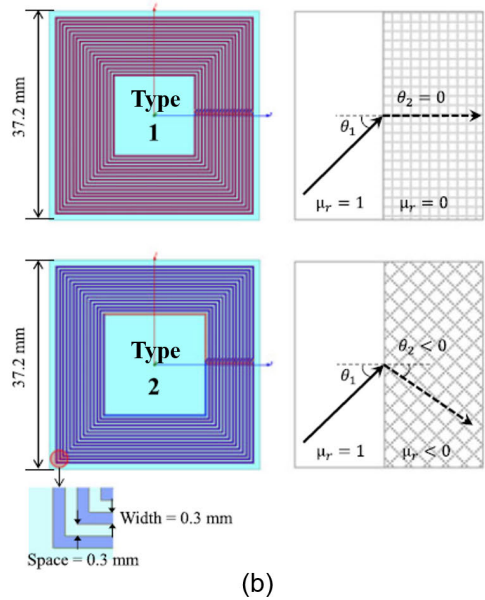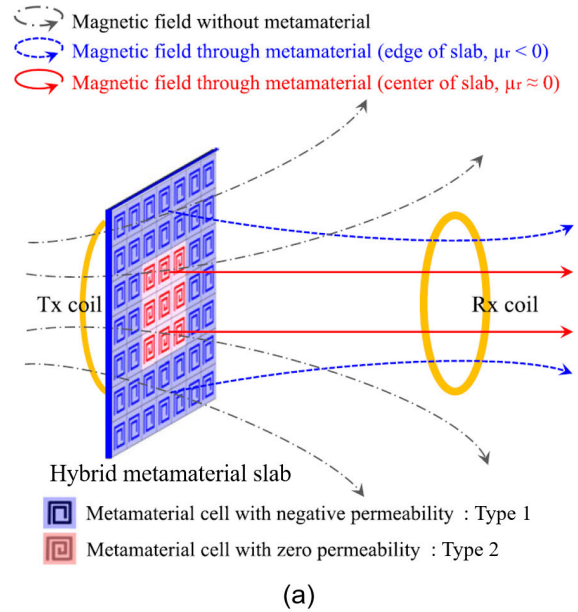

FIGURE 6. (a) Conceptual configuration of the WPT with the HMS. (b) Structure and refraction property of the two different metamaterial unit cells [56].

transfer distance between Tx and Rx coils of 15-30 cm and the location of the employed HMS at 3.5 cm in front of the Tx coil. As the additional structure positioned between the Tx and Rx coils is not preferred for the practical WPT system, the HMS has been positioned nearby the Tx. The PTE of the HMS incorporated system shows improvements from 35.3 % to 41.7 % at the distance of 10 cm and from 10.7 % to 18.6 % at the distance of 20 cm. Meanwhile, the PTE peak is shifted to a higher frequency region due to the mutual coupling between the MTM and the spirals. Also, Lee *et al.* [58] have introduced a two-stacked HMS in their following work. The two-stacked HMS has been placed in front of the

Tx with a gap of 1 cm between slabs. When the two-stacked HMS is employed to the WPT system, the PTE of the system improves from 23.9 % to 49.3 % at the distance of 15 cm and from 6.9 % to 29.4 % at the distance of 20 cm. Even though these studies have shown the advantages of HMS slab, further studies are needed for the proof of the concept. For example, if the MTM unit cells with different negative refraction index are properly positioned in HMS slab, the magnetic fields can be focused to the desired direction meaning the direction of the magnetic fields can be changed according to the combination of different MTM unit cells. These studies can be a new regime of the MTM-based WPT systems.

B. METAMATERIAL-BASED WPT FOR A MISALIGNMENT COMPENSATION

In WPT systems, misalignment between Tx and Rx coils is one of the critical factors that determines the PTE of the WPT systems. Any misalignment in WPT systems from the initial optimal location results in significant degradation in PTE [70]. In order to address this issue, many studies have been conducted to compensate the misalignment conditions in the WPT systems.
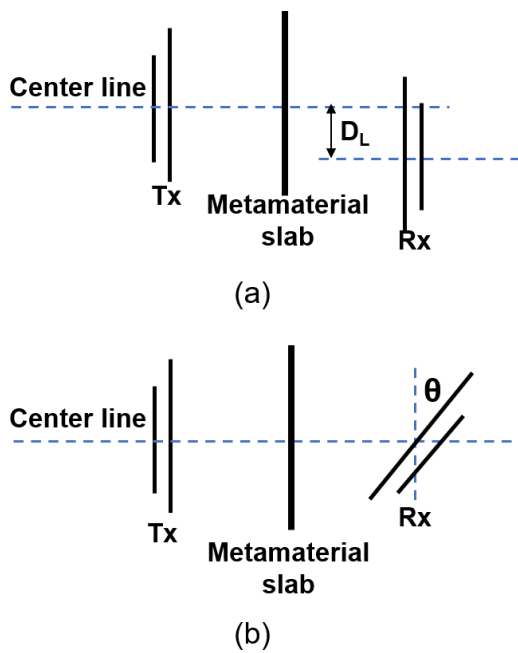

FIGURE 7. Misaligned conditions in the WPT system with metamaterial slab: (a) lateral misalignment with D_L (b) angular misalignment with θ.

Some researchers have investigated that the MTMs can mitigate the PTE degradation caused by the misalignment owing to the MTMs' evanescent wave amplification property [43], [44], [53]. In general, misalignment conditions in the WPT systems can be divided into two categories which are lateral misalignment (D_L) and angular misalignment (θ), as shown in Fig. 7. Recently, the impact of the lateral and angular misalignments on the WPT system and the compensation of the PTE in the misaligned WPT system with the
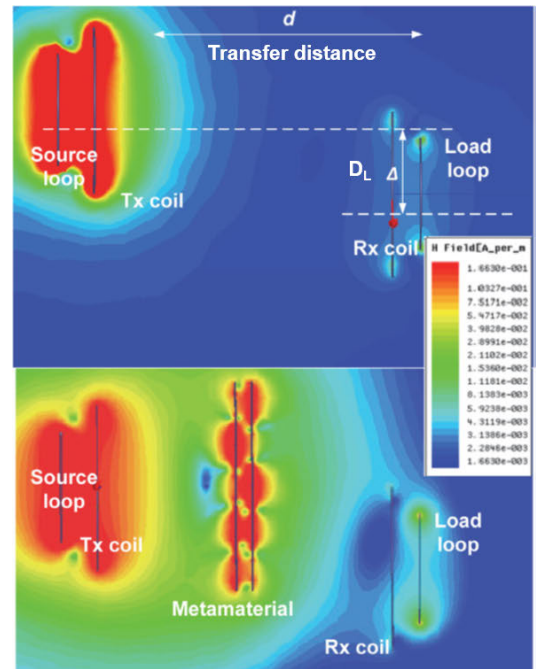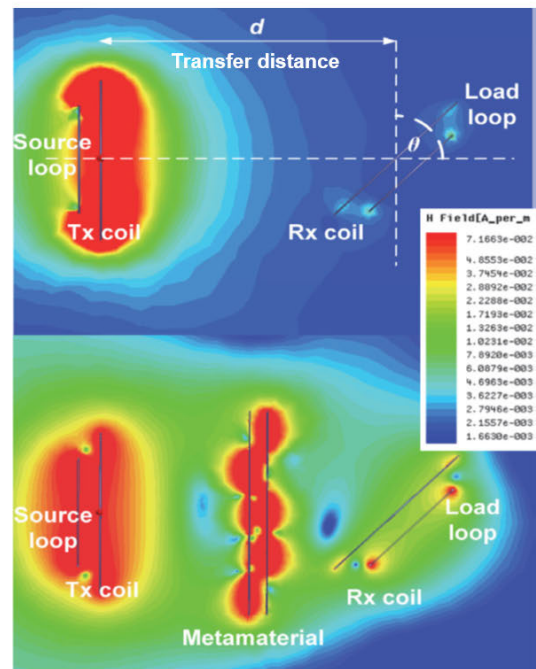

**FIGURE 8.** Magnetic field distribution of the WPT system with and without metamaterial slab (a) under a lateral misalignment (D_L) of 30 cm (b) under an angular misalignment (θ) of 45° [43].

MTM slab have been reported in [43]. Fig. 8 shows the magnetic field distribution of the WPT system with and without MTM slab under a lateral misalignment (D_L) of 30 cm and an angular misalignment (θ) of 45° with a transfer distance of d = 100 cm and a resonant frequency of 6.6 MHz. The

simulation results in Fig. 8 show that the MTM slab amplifies the evanescent waves leading to an increase in the magnetic coupling between the Tx and Rx coils for both lateral and angular misalignment conditions. The experimental results show that the MTM slab can improve the PTE of the WPT system and compensate the impacts of the misalignments on the WPT system. At the transfer distance of d = 100 cm, the PTE of the WPT system with MTM slabs improves from 25.3 % to 57.9 % in an aligned condition. Under the lateral misalignment condition, the PTE of the WPT system with MTM slabs shows an improvement by 33.1 % and 27.3 % at D_L = 10 cm and 40 cm, respectively. As for the angular misalignment condition, the PTE improves by 32.9 % and 30.9 %, at θ = 15° and 45°, respectively.
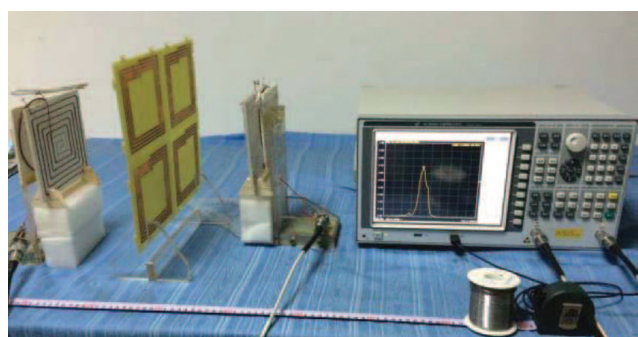
(a)
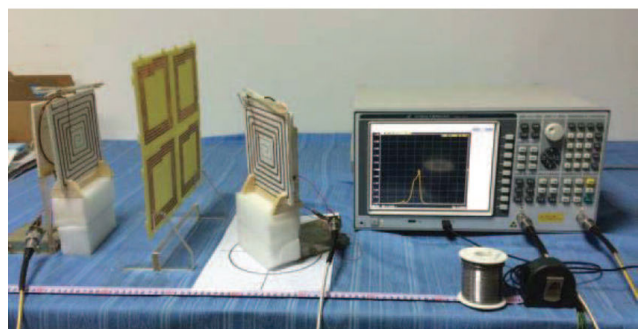
(b)

FIGURE 9. Experimental setup of the WPT system with metamaterial slab: (a) lateral misalignment condition (b) angular misalignment condition [44].

Chen and Tan [44] also have utilized same methodology with [43] to verify the effectiveness of the MTM slab for the WPT in the lateral and angular misaligned conditions, as shown in Fig. 9. The MTM slab which consists of 2 × 2 MTM unit cells has been positioned between Tx coil and Rx coils to mitigate the misalignment condition. The measurement results show that the PTE of the WPT system with a MTM slab improves from 7.8 % to 45.8 % at the transfer distance of d = 30 cm and D_L = 6 cm. As for the angular misalignment condition, the PTE improves by 35.3 % and 31 %, at θ = 30° and 45°, respectively.

The work referenced in this section has proved that the metamaterial slab effectively compensates the effects of the

misalignments on the WPT system and offers more practical ways for electronic charging devices with increased misalignment torelance.
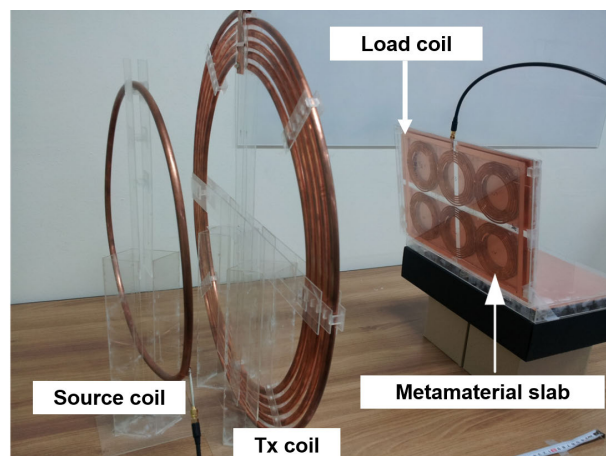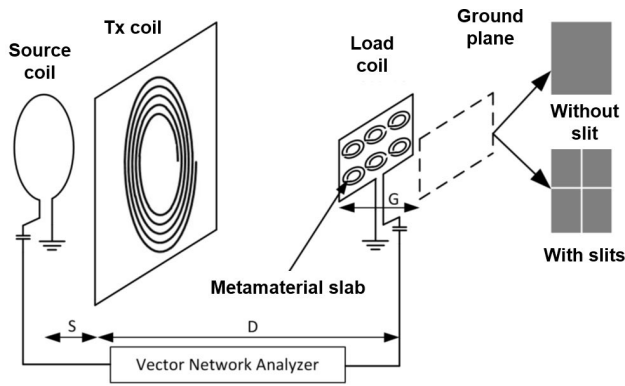

FIGURE 10. Three-coil WPT system with metamaterial slab for laptop application [55].

C. METAMATERIAL-BASED WPT FOR CONSUMER ELECTRONICS

In consumer electronics research, WPT is very important as it provides portability and convenience to users. Recently, Nguyen *et al.* [55] have demonstrated a three-coil WPT system with the MTM slab in order to improve the transfer efficiency for laptop applications. As shown in Fig. 10, the proposed three-coil WPT system has a planar load coil so that it can be applied to planar consumer electronic devices, such as mobile phones and laptops, etc. This WPT system has been designed to operate at 6.78 MHz, an AirFuel Alliance Standard frequency. In corresponding experiment results, the PTE of the WPT system with a MTM slab is improved by 27 % at a distance of 50 cm.

In general, most consumer electronic devices have one or more ground planes. Taking this situation into account, the ground plane has been placed behind the load coil with a gap G, as shown in Fig. 11. (a) and the impact of the ground plane on the PTE of the WPT system has been investigated for several cases as follows: 1) With and without the MTM slab, 2) Ground plane with and without slit, 3) The gap G = 0.2 cm and G = 2 cm. As depicted in Fig. 11. (b), when the G is small and there is no slit on the ground, the PTE of the WPT shows the lowest value. The reason is that most of the magnetic fields are reflected due to the ground plane. On the other hand, improved PTE could be achieved for the entire distance by increasing the gap to 2 cm or making slits on the ground plane. The maximal improvement of transfer efficiency achieved by changing the gap and slit size has been about 55 % at the transfer distance D = 20 cm. It is possible to mitigate the ground impact by increasing the gap and/or making slits on the ground plane.

(a)
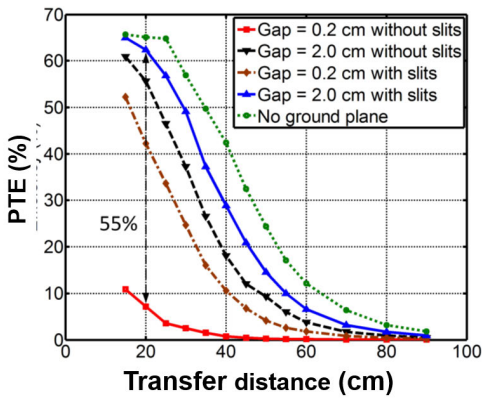
(b)

FIGURE 11. (a) Schematic of a three-coil WPT system with metamaterial slab and ground plane (unit: cm) (b) Investigation of the ground impact on PTE of the WPT with metamaterial slab [55].

Moreover, in order to address the practical WPT system for laptop applications, a laptop model with a screen and a keyboard has been implemented and the impacts of the load coil angle and position have been investigated. The ground plane is inserted to the screen and keyboard and the angles of the screen are 45°, 90°, and 135°, relative to the keyboard. The PTE with the angle of 90° has shown the highest PTE since the magnetic field coupled to the load coil becomes maximum at this angle. Meanwhile, the PTE with an angle of 45° has shown the lowest. As for the impact of the load coil position, it has been shown that the highest PTE is 51 % when the distance from the center of the Tx is 15 cm. This study has shown the MTM -based WPT system for consumer electronics and explored various experiments for practical applications.

D. HIGH DIELECTRIC/PERMITTIVITY METAMATERIAL-BASED WPT

In the field of the MTM-based WPT systems, the studies have been mainly focused on the negative permeability MTM slab which reflects the negative refraction property. Most of the negative permeability MTM slabs in the WPT applications are realized by an array of copper-based MTM unit cells.

Alternatively, a way to achieve a single or double negative MTMs by using very high dielectric materials has been studied [71]. In addition, several theoretical analyses have been reported that the single or double negative MTMs can be obtained by high dielectric spheres [72], [73] or cylindrical structures [75] based on the Mie resonance theory which is the theory of electromagnetic plane wave scattering by a dielectric sphere [76], [77]. The Mie resonances of dielectric inclusions provide a different mechanism for the creation of electric or magnetic resonance and offer more various routes for the fabrication of MTMs [78].
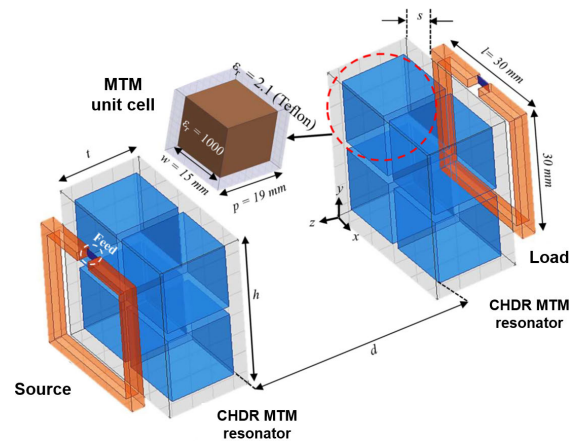

FIGURE 12. Schematic of the CHDR MTM-based WPT system [64].

Recently, Das *et al.* [64] have proposed the WPT system based on a cubic high-dielectric resonator (CHDR) MTM. As shown in Fig. 12, the WPT system consists of a source coil, a load coil, and two CHDR MTM resonators. The CHDR MTM resonators are placed in front of the source and load coils with a distance of 4 mm. The CHDR MTM-based WPT system has been simulated and characterized using High Frequency Structure Simulator (HFSS, Ansys Inc.). In the simulation, the CHDR MTM is composed of periodic 2×2 arrays of high-dielectric elements ($\varepsilon_r = 1000$) in a low-dielectric constant Teflon background ($\varepsilon_r = 2.1$). The simulated resonant frequency is $f = 476.8 MHz$. In Fig. 13, the refractive index, n, the value of the relative permittivity, ε_r, the value of the relative permeability, μ_r, are extracted from the simulation results (S_{11}, S_{21}) by using the standard retrieval methods [75]–[77]. The region covered by the blue rectangular box is the negative refractive index region. In this region, the real values of both ε_r and μ_r are negative. Therefore, the CHDR MTM resonator realizes the properties of the DNG MTMs in this region. As for the implementation of the CHDR MTM-based WPT system (Fig. 14), the CHDR cube has been fabricated using the EXXELIA TEMEX E5080 ceramic ($\varepsilon_r = 78$). The entire CHDR MTM consists of a 3×3 array and is excited by the source and load coils. The measured resonant frequency of the CHDR based-WPT system is 1.7 GHz which is higher than the simulated one because of the differences in the material and size of the CHDR MTM resonator. The measured PTE of the CHDR

based-WPT system is 52 % at the transfer distance of 3.6 cm. This study has shown a high permittivity MTM for the WPT system for the first time and proved its effectiveness. However, the CHDR MTM structure has had nonplanar and bulky structures, posing potential limitations in the practical applicability of its design.
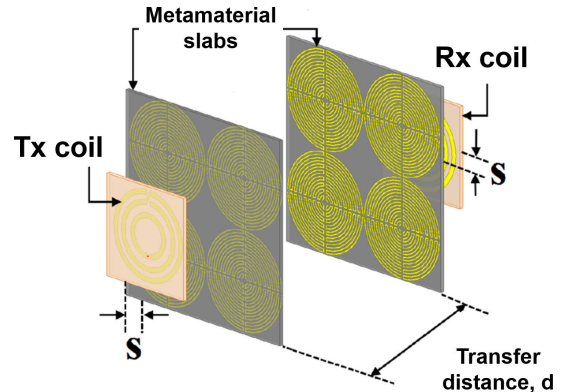

FIGURE 13. Extracted parameters of the CHDR MTM resonator. (a) Real relative permittivity. (b) Imaginary relative permittivity. (c) Real relative permeability. (d) Imaginary relative permeability [64].

FIGURE 14. Fabricated CHDR MTM-based WPT system [64].

Subsequently, Shaw and Mitra [53] have proposed a WPT system based on the high permittivity (HP) MTM instead of the high dielectric MTM. Due to its planar MTM structures, the design limitations caused by the nonplanar and bulky structures can be resolved. In order to realize the high permittivity property of the MTM, a compact low-loss circular spiral split-ring resonator structure has been utilized. As shown in Fig. 15, the WPT system consists of a Tx coil, an Rx coil, and two HP MTM slabs. The 2×2 HP MTM slabs are located in front of the Tx and Rx coils with spacing s. The high permittivity property of the MTM slabs is simulated and

FIGURE 15. Schematic of the HP MTM-based WPT system [53].

characterized using HFSS. The simulated S_{11} and S_{21} of the HP MTM unit cell are shown in Fig. 16 (a). The Kramers–Kronig retrieval method [82] is used for extracting the relative permittivity, which is shown in Fig. 16 (b). The blue region in the figure shows the operating zone for the PTE improvement of the WPT system, where the real part of the permittivity is high while the imaginary part is only about 0.47 reflecting the low loss of the MTM. For the proof of concept, prototypes have been fabricated, and measured, as shown in Fig. 17. The operating frequency of the WPT system is around 472.6 MHz. As the high permittivity property of MTMs has enhanced the magnetic coupling, the PTE of the WPT system with the HP MTM slabs has increased compared to the WPT system without the HP MTM slabs. At a transfer distance of 30 mm, the improved PTEs achieved from the measurement as well as from simulation with the insertion of the HP MTM slabs are 8.6 % and 9.1 %, respectively (Fig. 18).
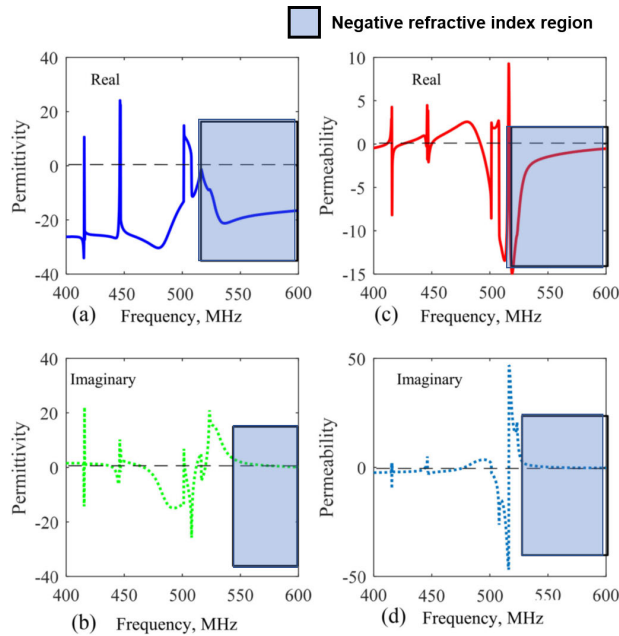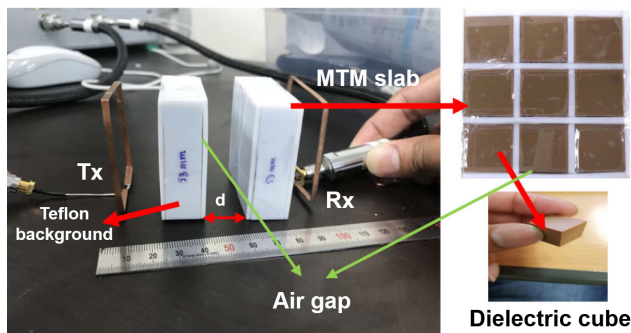

FIGURE 16. (a) Characteristics of S_{11} and S_{21} of the HP MTM unit cell (b) Extracted real and imaginary values of the relative permittivity [53].

The work referenced in this section has demonstrated that the high dielectric/permittivity MTM slabs are effective in improving the PTE of the WPT systems and contribute to expanding the research area of the MTM-based WPT systems.

E. COMPARISON OF THE PREVIOUSLY REPORTED METAMATERIAL-BASED WPT SYSTEMS
In order to have a comprehensive understanding of the MTM-based WPT systems, the characteristics of previously

TABLE 1. Comparison of the previously reported metamaterial (MTM) based WPT systems.

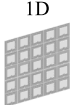| Ref.	Categorization		Configuration of the MTM /# of MTM slabs	Operating frequency (MHz)	Diameter of Tx/Rx coils (mm)	Property of MTM	Transfer distance (mm)	Normalized transfer distance	PTE / PTE improvement with MTM (%)	Figure of merit
[33]	1D	Middle	Square spiral resonator (double sided) / 2	27	400	$\mu_r = -1$	500 (0.045λ)	2.5	47 / 30	0.59
[34]			Square spiral resonator (double sided) / 1	4	Tx=90 Rx=40	$\mu_r = -1$	100 (0.0013λ)	3.33	22 / 21.3	0.37
[35]			Square spiral resonator (double sided) / 1	6.78	150	$\mu_r = 0$ $\mu_r = -1.8$	200 (0.0045λ)	2.67	47 / 38.3 (Sim.)	0.63
[36]			Hexagon spiral resonator (double sided) / 1	6.78	150	Negative μ_r	200 (0.0045λ)	2.67	38 / 17	0.51
			Hexagon spiral resonator (double sided) / 2	6.78	150	Negative μ_r	200 (0.0045λ)	2.67	51 / 30	0.68
[37]			Circular spiral resonator (double sided) / 1	58.8	60	$\mu_r = -1$	200 (0.039λ)	6.67	13.58 / 10.22 (Sim.)	0.45
[38]			Square spiral resonator (double sided) / 1	13.56	100	$\mu_r = -0.053$	300 (0.0136λ)	6	13.4 / 10.5 (Sim.)	0.4
[39]			Circular spiral resonator (single sided) / 1	6.5	600	Negative μ_r	1,000 (0.0217λ)	3.33	35 / 15.1	0.58
			Circular spiral resonator (single sided) / 2	6.5	600	Negative μ_r	1,000 (0.0217λ)	3.33	54.3 / 34.4	0.9
[40]			Square spiral resonator (single sided) / 1	2.8	500	$\mu_r = -1.1$	1,600 (0.015λ)	6.4	50.92 / 18.58	1.6
[41]			Square spiral resonator (single sided) / 1	13.56	100	Negative μ_r	300 (0.0136λ)	6	52.3 / 41.7	1.57
[42]			Meander line (single sided) / 1	27.4	400	Negative μ_r	200 (0.0183λ)	1	41.2 / 10.7	0.21
[43]			Circular spiral resonator (single sided) / 2	6.5	600	Negative μ_r	1,000 (0.0217λ)	3.33	57.9 / 32.6	0.96
[44]			Square spiral resonator (single sided) / 1	13.56	130	$\mu_r = -1.1$	300 (0.0136λ)	4.62	45.8 / 36.4	1.06
[67]			Square spiral resonator (double sided) / 2	6.78	500	$\mu_r = -1$	600 (0.0136λ)	2.4	36.7 / 20.7	0.44
[45]		Middle & Front	Square spiral resonator (double sided) / 1	17.6	60	$\mu_r = -1$	200 (0.0117λ)	6.67	3.9 / 3.5	0.13
[46]			Square spiral resonator (double sided) / 1	6.78	150	$\mu_r = -0.1$	200 (0.0045λ)	2.67	54.9 / 44.2	0.73
[47]			Circular spiral resonator (double sided) / 1	26.65	Tx=50 Rx=36	$\mu_r = -1$	79 (0.007λ)	3.72	18.23 / 6.93	0.34
[48]			Square spiral & meander line resonator (double sided) / 3	14.6	185	Negative μ_r	500 (0.0244λ)	5.4	50 / - (Sim.)	1.35
[49]			Square spiral & meander line resonator (double sided) / 3	14.6	70	Negative $\mu_r,$ and ε_r	140 (0.0068λ)	4	30.9 / 30.85	0.6
[50]			Square spiral resonator (double sided) / 1	6.78	140	$\mu_r = -0.8$	150 (0.0034λ)	2.14	22.4 /16.86	0.24

TABLE 1. *(Continued.)* Comparison of the previously reported metamaterial (MTM) based WPT systems.

| Ref.	Categorization			Configuration of the MTM /# of MTM slabs	Operating frequency (MHz)	Diameter of Tx/Rx coils (mm)	Property of MTM	Transfer distance (mm)	Normalized transfer distance	PTE / PTE improvement with MTM (%)	Figure of merit
[51]	1D	Middle & Back		Circular ring resonator (single sided) / 2	2,600	66.5	High S_{21} MTM & high S_{11} reflector	25 (0.2168λ)	0.75	70.64 / 10.49	0.26
[52]				Square spiral resonator (single sided) / 3	13.56	200	Near zero and negative μ_r	400 (0.0181λ)	4	48.3 / 12.06	0.96
[53]		Front		Split ring resonator (single sided) / 2	472.6	18	High ε_r	30 (0.0473λ)	3.33	60.8 / 8.6	1.02
[54]				Square spiral resonator (double sided) / 1	6.78	Tx=170 Rx=60	$\mu_r = 0$	150 (0.0034λ)	1.5	45.2 / 38.1	0.34
[55]				Circular spiral resonator (single sided) / 1	6.78	300	-	350 (0.0079λ)	2.33	50 / 27	0.58
[56]				Square spiral resonator (double sided) / 1	7.43	150	$\mu_r = 0$ $\mu_r = -1$	200 (0.005λ)	2.67	18.6 / 7.9	0.25
[57]				Square spiral resonator (double sided) / 1	5.77	42	-	25 (0.0005λ)	1.19	12 / 7	0.07
[58]				Square spiral resonator (double sided) / 2	6.86	150	$\mu_r = 0.06$ $\mu_r = -1.3$	200 (0.0046λ)	2.67	29.4 / 22.5	0.39
[65]		Back		Artificial perfect magnetic conductor / 2	24.1	170	-	400 (0.0322λ)	4.7	72 / 24	1.69
[66]		Side		Square spiral resonator (double sided) / 2	7	140	$\mu_r = -1$	225 (0.0053λ)	3.21	16.24 / 15.7	0.26
[59]	2D	Middle		Square spiral resonator (single sided) / 1	2.65	42.5	$\mu_r = -1$	122 (0.001λ)	5.74	50 / 17	1.43
[67]				Square spiral resonator (double sided) / 1	6.78	500	$\mu_r = -1$	600 (0.0136λ)	2.4	25 / 9	0.3
[60]	3D	Middle		Square spiral resonator (single sided) / 1	8.64	400	Negative μ_r	1,000 (0.0288λ)	5	53.3 / 24.5	1.33
[61]				Ferrite loaded solenoid (3D structure) / 1	5.57	40	$\mu_r = -1$	40 (0.0007λ)	2	35 / 15	0.35
[62]				Circular spiral resonator (double sided) / 1	6.5	600	$\mu_r = -1$	1,000 (0.0217λ)	3.33	54 / 33	0.9
[63]				Square spiral resonator (double sided) / 1	13-16	20	Negative μ_r	80 (0.0039λ)	8	1 / 0.99999	0.04
[67]				Square spiral resonator (double sided) / 1	6.78	500	$\mu_r = -1$	600 (0.0136λ)	2.4	40 / 24	0.48
[64]	3D	Front		Cubic high dielectric resonator (3D structure) / 2	1,700	30	Negative $\mu_r, and\ \varepsilon_r$	36 (0.2042λ)	2.4	52 / -	0.62
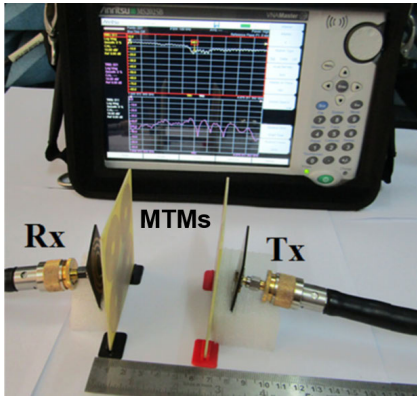
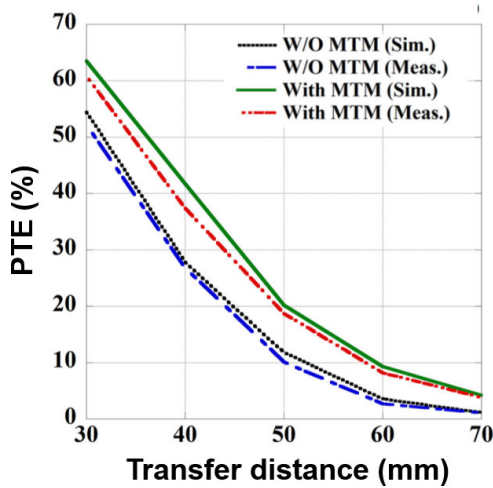**FIGURE 17.** Experimental setup for the HP MTM-based WPT system [53].

FIGURE 18. Simulated and measured PTE of the HP MTM-based WPT system [53].

reported MTM-based WPT systems are summarized and compared in Table 1. The categorization of the reference MTM-based WPT systems is based on Fig. 3 in terms of configuration of the MTM, the location of the slabs, and the number of the MTM slabs. Comparison parameters include the operating frequency, Tx / Rx coils diameters, the property (or type) of the MTM, the transfer distance, and the PTE / PTE improvement with MTM. As the experiments of each paper accommodates different coil sizes, which impacts the PTE as a function of distance, for fair comparison, the transfer distance between Tx and Rx coils has been normalized to the geometrical mean of Tx and Rx coil radii as shown in Eq. (17) [83].

$$Normalized\ transfer\ distance = \frac{Transfer\ distance}{\sqrt{r_T \cdot r_R}} \quad (17)$$

where r_T and r_R are the Tx radius, and Rx radius, respectively. Additionally, a figure of merit (FoM) has been introduced to compare all those WPT systems taking into account the transfer distance, the coil size, and the PTE. The equation for

the FoM is as follows [84]:

$$FoM = \frac{Transfer\ distance}{Diameter\ of\ coil} \times PTE \quad (18)$$

This table is expected to provide an overview of contemporary techniques used for the MTM-based WPT systems, and important parameters.

Furthermore, the PTEs of the previously reported MTM-based WPT systems are plotted as a function of the normalized transfer distance as a white space chart, as shown in Fig. 19. The reference works cover frequencies from 2.65 MHz up to 2.7 GHz while frequency categorization has been based on the AirFuel Alliance Standard frequency system at 6.78 MHz, on which emphasis is placed in this review. Even though it is hard to compare these works directly due to the variety of topologies and types of the MTMs and the WPT systems, this is expected to provide a quick reference for engineers and researchers working on the MTM based WPT systems. In Fig. 19, it is shown that as the normalized transfer distance increases, the PTE tends to decrease, except for a few cases. This tendency is related to the decrease of the magnetic coupling between the Tx coil, Rx coil, and the MTM slab due to the increase of the normalized transfer distance between them, which follows the fundamental physics. Meantime, the comparison table and figure in this section enlist the concurrent state-of-the-art MTM-based WPT systems and are expected to assist the researchers by providing them with some important parameters of the MTM-based WPT systems to achieve better PTE.

IV. PERSPECTIVES AND CHALLENGES OF THE METAMATERIAL-BASED WPT SYSTEMS

It has been shown that the PTE and transfer distance of the WPT systems can be greatly improved by incorporating the MTMs in the system, which is attributed to the negative refraction and evanescent wave amplification properties of the MTMs. Without any doubt, the development of MTMs will further boost the progress of the WPT systems. However, investigations on the applications of the MTMs based WPT systems are still in an early stage. Thus, here several perspectives and challenges of the MTM based WPT systems for future progress are discussed.

First, as the PTE is one of the most important merit parameters of the WPT systems, the insertion loss of the MTM slab should be minimized. Even though the inserted MTM slab improves the PTE of the WPT systems, it inevitably experiences insertion losses in practical WPT systems. Chabalko *et al.* [59] have investigated the insertion loss of the MTM slabs and single turn resonator which are inserted between Tx and Rx coils. They show that the single turn resonator can significantly increase the PTE of the WPT system in a certain case even more than MTM slab. The reason for this phenomenon is that the insertion loss of the MTM slab is much larger than that of the single turn resonator due to the complex structure of the MTM slab and the non-optimized raw material selection for the MTM. Given this, the structure
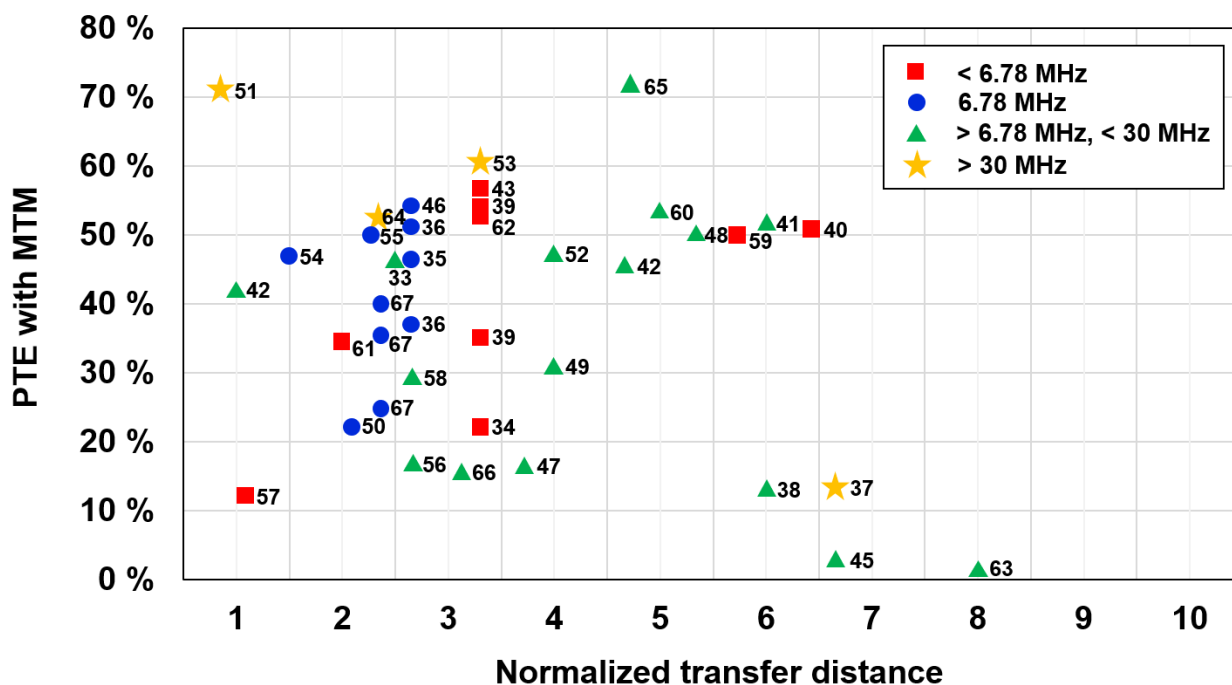
FIGURE 19. The PTEs of the previously reported metamaterial-based WPT systems in terms of normalized transfer distance.

of the MTM slab should be carefully designed in order to minimize the added insertion loss. Moreover, if the insertion loss owing to the conductor loss or substrate loss of the MTM slab can be reduced, it will provide great potentials to improve the PTE of the WPT systems. Wang *et al.* [37] have demonstrated the superconductor based MTM slab with low conductor loss. It is shown that the lower loss properties of the superconductor incorporated with the properties of MTMs can improve more the PTE of the WPT systems effectively. On the other hand, it has been reported that the negative refraction property could be realized without using such bulky structures [85]. Since a thick substrate could add an additional substrate loss, a thinner MTM slab should be preferably used in order to minimize the insertion loss of the MTM slab. As the insertion loss of the MTM slab directly impacts the PTE of the WPT systems, lowering it down must be of prime design concern, which is expected to provide great potentials to improve the PTE of the WPT systems and therefore it should be further investigated. In addition, there are additional losses which can affect the PTE when it comes to the final applications. In general, the MRC-based WPT systems consist of a power supplier, power amplifier, WPT resonators, rectifier, DC-DC converter, and load, etc. The losses in each step and unpredictable parameter changes (load, transfer distance, and orientation etc.) in WPT environments greatly affect the end to end PTE [86]. Thus, in order to achieve high efficiency MTM-based WPT systems, the efficiency of each step should be optimized and the entire WPT system needs to have an adaptability to various WPT environments.

Although the MTMs can improve the PTE of the WPT systems due to their unique properties, the studies on the MTM-based WPT systems for practical applications are still in the basic research stage yet. As the research and development activities of the WPT systems are actively executed in the broad fields and applications such as charging the portable electronic devices [87], electric vehicles or transportation equipment [88]–[90], and bio-medical implants [91]–[93], etc., much efforts should be exerted to develop practical MTM-based WPT systems. It is worth to notice that most of the reported MTM slabs have a bulky and thick structure, placing constraints toward their practical applications. It may not be practical if the additional bulky MTM slab is placed in the power transmission path, which would restrict the usefulness and flexibility of the WPT systems even being worse than the traditional wire charging systems. The possible approaches to address these issues are as follows. First, the MTM slab can be embedded in the WPT systems. For this approach, the optimization of the embedding position of the MTM slab should be studied in the future. Second, it could be embedding the MTM to the intermediate objects that do not interfere with users. Recently, Zheludev and Kivshar [94] have demonstrated an MTM-based smart table for the WPT system. The proposed MTM-embedded table increases the PTE regardless of the position of Tx and Rx if they are placed anywhere on the smart MTM table. This work showed the new possibility of practical MTM-based WPT systems. Further studies on the MTM-based WPT systems using embedded schemes should be addressed in the future for real implementations. Alternatively, it can be considered

to change the form factor or shape of the MTM slab. If the flexible or foldable MTM screen is inserted to the middle of the WPT systems and the screen can be rolled up e.g. onto the ceiling when not used, it does not require any designated space for the screen solving the aforementioned problem. In addition, modern WPT systems need to be compliant with the technology trend of reduced size, weight, and power (SWaP). Especially for the efficient usage of the space, the modern electronics transform their form factors to be deformed, rolled, and folded, e.g. rollable TVs and foldable phones without compromising the performance of the electronic systems. If this trend can be addressed in the MTM-based WPT systems while being compliant with the commercial WPT standards, it can take one step closer to the practical applications toward the efficient usage of the space.

Another thing to be considered is the trend of the MTM devices. Recently, active MTMs which can tune their properties in response to an external input have been studied [95]–[97]. Conventional MTMs, called passive MTMs, have fixed parameters once being made which limit the applications of MTM devices. In most of previous studies, the properties of the MTMs can not be changed once being fabricated as they adopt the passive MTMs. For the same reason, the operating frequency of the MTM slab is also fixed. Recently, the active MTMs have been studied in the field of the MTM-based WPT systems [98], [99]. Ranaweera *et al.* [99] have proposed an active MTM for dynamically field localizing WPT systems which can provide controlled and selective power transfer into the intended zone (hot zone). The hot zone can be realized using defect cavities created on the MTM unit cells which have switchable resonant frequencies. By realizing the enhanced fields on the intended region, both PTE and safety can be improved. However, the transfer distance has been limited as they have utilized the non-resonant loops for Tx and Rx coils. Moreover, no exhaustive investigation on the transfer distance which is one of the important parameters of the WPT systems has beenperformed. Even though they have shown the effectiveness of the active MTM in the field of WPT systems, further studies are needed for active MTM-based WPT systems. Especially, the studies on the negative refraction property of the active MTMs can be one of the candidates. If the negative refraction property of the MTM slab can be tuned, the direction of the magnetic fields can be also changed in response to the environments of the WPT. For example, when the Rx coil is misaligned to the Tx coil, the active MTM slab can effectively change the direction of the magnetic fields to the location of the Rx as the negative refraction index of MTM slab can be tuned. If the negative refraction property of the MTM unit cells can be modulated, an improved flexibility of the MTM-based WPT systems can be achieved and its applicability will be enlarged. It is expected that the active MTMs will give new opportunities for practical MTM-based WPT systems in various situations such as misaligned conditions or asymmetric WPT environments.

On the other side, in order to move further into the practical application of the MTM-based WPT systems, human safety should be carefully considered. In general, the specific absorption rate (SAR) value has been utilized to verify whether the designed devices are appropriate for practical applications and compliant with the safety limit or not. According to the IEEE C95.1-1999 standard, the average SAR over 1g of tissue model in cubic shape should be $\leq$1.6 W/kg for human safety [100]. For this reason, the investigation of the SAR analysis on the MTM-based WPT systems should be conducted. Recently, some researchers have demonstrated the MTM-based WPT systems for biomedical applications and showed the improved PTE in both the air and implantable environments of the WPT system using the properties of MTM [101]–[103]. Among them, Shaw and Mitra [101] provided the SAR analysis of the implantable WPT system with and without MTM slab. Even though the SAR analysis for human safety is a necessary step for the practical WPT systems, most of the MTM-based WPT systems have not taken into consideration the human safety issue yet.

V. CONCLUSION
This article has reviewed recent progress on the MTM and its application to WPT technologies. Brief history and fundamental of the MTM and WPT systems have been reviewed. Some of the remarkable and state-of-the-art concurrent works and their features have been highlighted including the improvement of the PTE, the compensation of the misalignment conditions, the application to the consumer electronics, and the usage of the high dielectric/permittivity MTMs. In order to provide a comprehensive outlook of the MTM-based WPT systems, the previously reported MTM-based WPT systems have been compared in terms of various parameters such as the MTM configuration, the MTM's position, the operating frequency, the WPT distance, and the PTE. The PTEs of these systems have been plotted as a function of the normalized transfer distance. This review is expected to provide an insight for understanding the trends of the MTM-based WPT system technologies and serve as a quick reference in the WPT research field. Also, the prospective and challenges of the MTM-based WPT systems have been discussed toward the advancement of the technology itself and the practical applications.

REFERENCES
[1] N. Tesla, "Apparatus for transmitting electrical energy," U.S. Patent 1 119 732 A, Dec. 1, 1914.
[2] W. C. Brown, "The history of power transmission by radio waves," *IEEE Trans. Microw. Theory Techn.*, vol. MTT-32, no. 9, pp. 1230–1242, Sep. 1984.
[3] A. Kurs, R. Moffatt, and M. Soljačić, "Simultaneous mid-range power transfer to multiple devices," *Appl. Phys. Lett.*, vol. 96, no. 4, Jan. 2010, Art. no. 044102.

[4] S. Maslovski, S. Tretyakov, and P. Alitalo, "Near-field enhancement and imaging in double planar polariton-resonant structures," *J. Appl. Phys.*, vol. 96, no. 3, pp. 1293–1300, Aug. 2004.

[5] Z. Chen, B. Guo, Y. Yang, and C. Cheng, "Metamaterials-based enhanced energy harvesting: A review," *Phys. B, Condens. Matter*, vol. 438, pp. 1–8, Apr. 2014.

[6] K. Sun, R. Fan, X. Zhang, Z. Zhang, Z. Shi, N. Wang, P. Xie, Z. Wang, G. Fan, H. Liu, C. Liu, T. Li, C. Yan, and Z. Guo, "An overview of metamaterials and their achievements in wireless power transfer," *J. Mater. Chem. C*, vol. 6, no. 12, pp. 2925–2943, 2018.

[7] B. Wang, W. Yerazunis, and K. H. Teo, "Wireless power transfer: Metamaterials and array of coupled resonators," *Proc. IEEE*, vol. 101, no. 6, pp. 1359–1368, Jun. 2013, doi: 10.1109/JPROC.2013.2245611.

[8] A. Sihvola, "Metamaterials in electromagnetics," *Metamaterials*, vol. 1, no. 1, pp. 2–11, Mar. 2007.

[9] V. G. Veselago, "The electrodynamics of substances with simultaneously negative values of and ϵ," *Sov. Phys. Uspekhi*, vol. 10, no. 4, pp. 509–514, Apr. 1968.

[10] K. Sun, Z.-D. Zhang, R.-H. Fan, M. Chen, C.-B. Cheng, Q. Hou, X.-H. Zhang, and Y. Liu, "Random copper/yttrium iron garnet composites with tunable negative electromagnetic parameters prepared by *in situ* synthesis," *RSC Adv.*, vol. 5, no. 75, pp. 61155–61160, 2015.

[11] N. Engheta and R. W. Ziolkowski, *Metamaterials: Physics and Engineering Explorations*. Hoboken, NJ, USA: Wiley, 2006.

[12] S. A. Ramakrishna, "Physics of negative refractive index materials," *Rep. Prog. Phys.*, vol. 68, no. 2, pp. 449–521, Feb. 2005.

[13] N. Engheta and R. W. Ziolkowski, "A positive future for double-negative metamaterials," *IEEE Trans. Microw. Theory Techn.*, vol. 53, no. 4, pp. 1535–1556, Apr. 2005.

[14] R. W. Ziolkowski, "Design, fabrication, and testing of double negative metamaterials," *IEEE Trans. Antennas Propag.*, vol. 51, no. 7, pp. 1516–1529, Jul. 2003.

[15] F. T. Ulaby and R. Umberto, *Fundamentals of Applied Electromagnetics*, 7th ed. 2014, p. 363.

[16] J. B. Pendry, "Negative refraction makes a perfect lens," *Phys. Rev. Lett.*, vol. 85, no. 18, pp. 3966–3969, Oct. 2000.

[17] J. Lu, T. M. Grzegorczyk, Y. Zhang, J. Pacheco, Jr., B.-I. Wu, J. A. Kong, and M. Chen, "Čerenkov radiation in materials with negative permittivity and permeability," *Opt. Express*, vol. 11, no. 7, pp. 723–734, Apr. 2003.

[18] H. F. Ma and T. J. Cui, "Three-dimensional broadband and broadangle transformation-optics lens," *Nature Commun.*, vol. 1, no. 1, p. 124, Dec. 2010.

[19] Z.-C. Shi, R.-H. Fan, Z.-D. Zhang, L. Qian, M. Gao, M. Zhang, L.-T. Zheng, X.-H. Zhang, and L.-W. Yin, "Random composites of nickel networks supported by porous alumina toward double negative materials," *Adv. Mater.*, vol. 24, no. 17, pp. 2349–2352, May 2012.

[20] M. J. Freire, R. Marques, and L. Jelinek, "Experimental demonstration of $\mu = -1$ metamaterial lens for magnetic resonance imaging," *Appl. Phys. Lett.*, vol. 93, no. 23, Dec. 2008, Art. no. 231108.

[21] Y. Huang, H.-J. Tang, E.-C. Chen, and C. Yao, "Effect on wireless power transmission with different layout of left-handed materials," *AIP Adv.*, vol. 3, no. 7, Jul. 2013, Art. no. 072134.

[22] V. A. Kalinin, K. H. Ringhofer, and L. Solymar, "Magneto-inductive waves in one two and three dimensions," *J. Appl. Phys.*, vol. 92, no. 10, pp. 6252–6261, 2002.

[23] A. A. Eteng, S. K. A. Rahim, C. Y. Leow, S. Jayaprakasam, and B. W. Chew, "Low-power near-field magnetic wireless energy transfer links: A review of architectures and design approaches," *Renew. Sustain. Energy Rev.*, vol. 77, pp. 486–505, Sep. 2017.

[24] R. E. Hamam, A. Karalis, J. D. Joannopoulos, and M. Soljačić, "Efficient weakly-radiative wireless energy transfer: An EIT-like approach," *Ann. Phys.*, vol. 324, no. 8, pp. 1783–1795, Aug. 2009.

[25] Y. Zhang, T. Lu, Z. Zhao, F. He, K. Chen, and L. Yuan, "Selective wireless power transfer to multiple loads using receivers of different resonant frequencies," *IEEE Trans. Power Electron.*, vol. 30, no. 11, pp. 6001–6005, Nov. 2015.

[26] H. Hoang, S. Lee, Y. Kim, Y. Choi, and F. Bien, "An adaptive technique to improve wireless power transfer for consumer electronics," *IEEE Trans. Consum. Electron.*, vol. 58, no. 2, pp. 327–332, May 2012.

[27] A. P. Sample, D. A. Meyer, and J. R. Smith, "Analysis, experimental results, and range adaptation of magnetically coupled resonators for wireless power transfer," *IEEE Trans. Ind. Electron.*, vol. 58, no. 2, pp. 544–554, Feb. 2011.

[28] T. P. Duong and J.-W. Lee, "Experimental results of high-efficiency resonant coupling wireless power transfer using a variable coupling method," *IEEE Microw. Wireless Compon. Lett.*, vol. 21, no. 8, pp. 442–444, Aug. 2011.

[29] J. Park, Y. Tak, Y. Kim, Y. Kim, and S. Nam, "Investigation of adaptive matching methods for near-field wireless power transfer," *IEEE Trans. Antennas Propag.*, vol. 59, no. 5, pp. 1769–1773, May 2011.

[30] T. C. Beh, M. Kato, T. Imura, S. Oh, and Y. Hori, "Automated impedance matching system for robust wireless power transfer via magnetic resonance coupling," *IEEE Trans. Ind. Electron.*, vol. 60, no. 9, pp. 3689–3698, Sep. 2013.

[31] F. Zhang, S. A. Hackworth, W. Fu, C. Li, Z. Mao, and M. Sun, "Relay effect of wireless power transfer using strongly coupled magnetic resonances," *IEEE Trans. Magn.*, vol. 47, no. 5, pp. 1478–1481, May 2011.

[32] B. Wang, T. Nishino, and K. Hoo Teo, "Wireless power transmission efficiency enhancement with metamaterials," in *Proc. IEEE Int. Conf. Wireless Inf. Technol. Syst.*, Honolulu, HI, USA, Aug. 2010, pp. 1–4.

[33] B. Wang, K. H. Teo, T. Nishino, W. Yerazunis, J. Barnwell, and J. Zhang, "Experiments on wireless power transfer with metamaterials," *Appl. Phys. Lett.*, vol. 98, no. 25, Jun. 2011, Art. no. 254101.

[34] Y. Z. Cheng, J. Jin, W. L. Li, J. F. Chen, B. Wang, and R. Z. Gong, "Indefinite-permeability metamaterial lens with finite size for miniaturized wireless power transfer system," *AEU Int. J. Electron. Commun.*, vol. 70, no. 9, pp. 1282–1287, Sep. 2016.

[35] Y. Cho, S. Lee, S. Jeong, H. Kim, C. Song, K. Yoon, J. Song, S. Kong, Y. Yun, and J. Kim, "Hybrid metamaterial with zero and negative permeability to enhance efficiency in wireless power transfer system," in *Proc. IEEE Wireless Power Transf. Conf. (WPTC)*, Aveiro, Portugal, May 2016, pp. 1–3.

[36] W. Xin, C. C. Mi, F. He, M. Jiang, and D. Hua, "Investigation of negative permeability metamaterials for wireless power transfer," *AIP Adv.*, vol. 7, no. 11, Nov. 2017, Art. no. 115316.

[37] X. Wang, Y. Wang, Y. Hu, Y. He, and Z. Yan, "Analysis of wireless power transfer using superconducting metamaterials," *IEEE Trans. Appl. Supercond.*, vol. 29, no. 2, pp. 1–5, Mar. 2019.

[38] C. Lu, X. Huang, C. Rong, Z. Hu, J. Chen, X. Tao, S. Wang, B. Wei, and M. Liu, "Shielding the magnetic field of wireless power transfer system using zero-permeability metamaterial," *J. Eng.*, vol. 2019, no. 16, pp. 1812–1815, Mar. 2019.

[39] A. L. A. K. Ranaweera, T. P. Duong, and J.-W. Lee, "Experimental investigation of compact metamaterial for high efficiency mid-range wireless power transfer applications," *J. Appl. Phys.*, vol. 116, no. 4, Jul. 2014, Art. no. 043914.

[40] C. Rong, X. Tao, C. Lu, Z. Hu, X. Huang, Y. Zeng, and M. Liu, "Analysis and optimized design of metamaterials for mid-range wireless power transfer using a class-E RF power amplifier," *Appl. Sci.*, vol. 9, no. 1, p. 26, Dec. 2018.

[41] J.-F. Chen, Z. Ding, Z. Hu, S. Wang, Y. Cheng, M. Liu, B. Wei, and S. Wang, "Metamaterial-based high-efficiency wireless power transfer system at 13.56 MHz for low power applications," *Prog. Electromagn. Res. B*, vol. 72, pp. 17–30, 2017.

[42] T. Shaw, A. Roy, and D. Mitra, "Efficiency enhancement of wireless power transfer system using MNZ metamaterials," *Prog. Electromagn. Res. C*, vol. 68, pp. 11–19, 2016.

[43] A. L. A. K. Ranaweera, C. A. Moscoso, and J.-W. Lee, "Anisotropic metamaterial for efficiency enhancement of mid-range wireless power transfer under coil misalignment," *J. Phys. D, Appl. Phys.*, vol. 48, no. 45, pp. 455104-1–455104-8, Nov. 2015.

[44] J. Chen and H. Tan, "Metamaterial for wireless power transfer system at 13.56 MHz with coil misalignment," in *Proc. 7th IEEE Int. Symp. Microw., Antenna, Propag., EMC Technol. (MAPE)*, Xi'an, China, Oct. 2017, pp. 313–317.

[45] Y. Zhang, H. Tang, C. Yao, Y. Li, and S. Xiao, "Experiments on adjustable magnetic metamaterials applied in megahertz wireless power transmission," *AIP Adv.*, vol. 5, no. 1, pp. 2075–2084, Jan. 2015.

[46] Y. Cho, J. J. Kim, D.-H. Kim, S. Lee, H. Kim, C. Song, S. Kong, H. Kim, C. Seo, S. Ahn, and J. Kim, "Thin PCB-type metamaterials for improved efficiency and reduced EMF leakage in wireless power transfer systems," *IEEE Trans. Microw. Theory Techn.*, vol. 64, no. 2, pp. 353–364, Feb. 2016.

[47] A. Rajagopalan, A. K. Ramrakhyani, D. Schurig, and G. Lazzi, "Improving power transfer efficiency of a short-range telemetry system using compact metamaterials," *IEEE Trans. Microw. Theory Techn.*, vol. 62, no. 4, pp. 947–955, Apr. 2014.

[48] C. Rong, C. Lu, Z. Hu, X. Huang, X. Tao, S. Wang, B. Wei, S. Wang, and M. Liu, "Analysis of wireless power transfer based on metamaterial using equivalent circuit," *J. Eng.*, vol. 2019, no. 16, pp. 2032–2035, Mar. 2019.

[49] Y. Fan, L. Li, S. Yu, C. Zhu, and C.-H. Liang, "Experimental study of efficient wireless power transfer system integrating with highly sub-wavelength metamaterials," *Prog. Electromagn. Res.*, vol. 141, pp. 769–784, 2013.

[50] C. Zhao, S. Zhu, H. Zhu, Z. Huang, and X. Luo, "Accurate design of deep sub-wavelength metamaterials for wireless power transfer enhancement," *Prog. Electromagn. Res. C*, vol. 83, pp. 195–203, 2018.

[51] A. Bhattacharya, T. Shaw, and D. Mitra, "Performance enhancement of wireless power transfer system by controlling transmission and reflection properties of metamaterials," in *Proc. IEEE MTT-S Int. Microw. RF Conf. (IMaRC)*, Kolkata, India, Nov. 2018, pp. 1–4.

[52] C. Lu, C. Rong, X. Huang, Z. Hu, X. Tao, S. Wang, J. Chen, and M. Liu, "Investigation of negative and near-zero permeability metamaterials for increased efficiency and reduced electromagnetic field leakage in a wireless power transfer system," *IEEE Trans. Electromagn. Compat.*, vol. 61, no. 5, pp. 1438–1446, Oct. 2019.

[53] T. Shaw and D. Mitra, "Wireless power transfer system based on magnetic dipole coupling with high permittivity metamaterials," *IEEE Antennas Wireless Propag. Lett.*, vol. 18, no. 9, pp. 1823–1827, Sep. 2019.

[54] H. Kim and C. Seo, "Highly efficient wireless power transfer using metamaterial slab with zero refractive property," *Electron. Lett.*, vol. 50, no. 16, pp. 1158–1160, Jul. 2014.

[55] V. T. Nguyen, S. H. Kang, J. H. Choi, and C. W. Jung, "Magnetic resonance wireless power transfer using three-coil system with single planar receiver for laptop applications," *IEEE Trans. Consum. Electron.*, vol. 61, no. 2, pp. 160–166, May 2015, doi: 10.1109/TCE.2015.7150569.

[56] Y. Cho, S. Lee, D.-H. Kim, H. Kim, C. Song, S. Kong, J. Park, C. Seo, and J. Kim, "Thin hybrid metamaterial slab with negative and zero permeability for high efficiency and low electromagnetic field in wireless power transfer systems," *IEEE Trans. Electromagn. Compat.*, vol. 60, no. 4, pp. 1001–1009, Aug. 2018.

[57] D. Brizi, J. P. Stang, A. Monorchio, and G. Lazzi, "A compact magnetically dispersive surface for low-frequency wireless power transfer applications," *IEEE Trans. Antennas Propag.*, vol. 68, no. 3, pp. 1887–1895, Mar. 2020.

[58] S. Lee, Y. Cho, S. Jeong, S. Hong, B. Sim, H. Kim, and J. Kim, "High efficiency wireless power transfer system using a two-stack hybrid metamaterial slab," in *Proc. IEEE Wireless Power Transf. Conf. (WPTC)*, London, U.K., Jun. 2019, pp. 616–619.

[59] M. J. Chabalko, J. Besnoff, and D. S. Ricketts, "Magnetic field enhancement in wireless power with metamaterials and magnetic resonant couplers," *IEEE Antennas Wireless Propag. Lett.*, vol. 15, pp. 452–455, 2016.

[60] J. Chen and H. Tan, "Investigation of wireless power transfer with 3D metamaterial for efficiency enhancement," in *Proc. 7th IEEE Int. Symp. Microw., Antenna, Propag., EMC Technol. (MAPE)*, Xi'an, China, Oct. 2017, pp. 309–312.

[61] E. S. Gamez Rodriguez, A. K. Ramrakhyani, D. Schurig, and G. Lazzi, "Compact low-frequency metamaterial design for wireless power transfer efficiency enhancement," *IEEE Trans. Microw. Theory Techn.*, vol. 64, no. 5, pp. 1644–1654, May 2016.

[62] A. L. A. K. Ranaweera, T. P. Duong, B. Lee, and J. Lee, "Experimental investigation of 3D metamaterial for mid-range wireless power transfer," in *Proc. IEEE Wireless Power Transf. Conf.*, Jeju, South Korea, May 2014, pp. 92–95.

[63] G. Lipworth, J. Ensworth, K. Seetharam, D. Huang, J. S. Lee, P. Schmalenberg, T. Nomura, M. S. Reynolds, D. R. Smith, and Y. Urzhumov, "Magnetic metamaterial superlens for increased range wireless power transfer," *Sci. Rep.*, vol. 4, no. 1, p. 3642, May 2015.

[64] R. Das, A. Basir, and H. Yoo, "A metamaterial-coupled wireless power transfer system based on cubic high-dielectric resonators," *IEEE Trans. Ind. Electron.*, vol. 66, no. 9, pp. 7397–7406, Sep. 2019.

[65] J. Wu, B. Wang, W. S. Yerazunis, and K. H. Teo, "Wireless power transfer with artificial magnetic conductors," in *Proc. IEEE Wireless Power Transf. (WPT)*, Perugia, Italy, May 2013, pp. 155–158.

[66] S. Zhu, C. Zhao, Z. Huang, Y. Zhang, and X. Luo, "Enhancement of wireless power transmission based on side-positioned metamaterials," in *Proc. IEEE PES Asia–Pacific Power Energy Eng. Conf. (APPEEC)*, Kota Kinabalu, Oct. 2018, pp. 241–245.

[67] W. Li, P. Wang, C. Yao, Y. Zhang, and H. Tang, "Experimental investigation of 1D, 2D, and 3D metamaterials for efficiency enhancement in a 6.78 MHz wireless power transfer system," in *Proc. IEEE Wireless Power Transf. Conf. (WPTC)*, Aveiro, Portugal, May 2016, pp. 1–4.

[68] A. Kurs, A. Karalis, R. Moffatt, J. D. Joannopoulos, P. Fisher, and M. Soljacic, "Wireless power transfer via strongly coupled magnetic resonances," *Science*, vol. 317, no. 5834, pp. 83–86, Jul. 2007.

[69] C. Moorey, W. Holderbaum, and B. Potter, "Investigation of high-efficiency wireless power transfer criteria of resonantly-coupled loops and dipoles through analysis of the figure of merit," *Energies*, vol. 8, no. 10, pp. 11342–11362, Oct. 2015.

[70] T. Duong and J.-W. Lee, "A dynamically adaptable impedance-matching system for midrange wireless power transfer with misalignment," *Energies*, vol. 8, no. 8, pp. 7593–7617, Jul. 2015.

[71] F. Zhang, Q. Zhao, L. Kang, J. Zhou, and D. Lippens, "Experimental verification of isotropic and polarization properties of high permittivity-based metamaterial," *Phys. Rev. B, Condens. Matter*, vol. 80, no. 19, Nov. 2009.

[72] L. Lewin, "The electrical constant of a material loaded with spherical particles," *J. Inst. Electr. Eng.*, vol. 94, no. 27, pp. 65–68, Jan. 1947.

[73] C. L. Holloway, E. F. Kuester, J. Baker-Jarvis, and P. Kabos, "A double negative (DNG) composite medium composed of magnetodielectric spherical particles embedded in a matrix," *IEEE Trans. Antennas Propag.*, vol. 51, no. 10, pp. 2596–2603, Oct. 2003.

[74] M. S. Wheeler, J. S. Aitchison, and M. Mojahedi, "Three-dimensional array of dielectric spheres with an isotropic negative permeability at infrared frequencies," *Phys. Rev. B, Condens. Matter*, vol. 72, no. 19, Nov. 2005.

[75] S. O'Brien and J. B. Pendry, "Photonic band-gap effects and magnetic activity in dielectric composites," *J. Phys., Condens. Matter*, vol. 14, no. 15, pp. 4035–4044, Apr. 2002.

[76] G. Mie, "Beiträge zur Optik trüber Medien speziell kolloidaler Metallösungen," *Ann. Phys.*, vol. 330, no. 3, pp. 377–445, 1908.

[77] L. Lewin, "The electrical constants of a material loaded with spherical particles," *J. Inst. Electr. Eng. III, Radio Commun. Eng.*, vol. 94, no. 27, pp. 65–68, Jan. 1947.

[78] Q. Zhao, J. Zhou, F. Zhang, and D. Lippens, "Mie resonance-based dielectric metamaterials," *Mater. Today*, vol. 12, no. 12, pp. 60–69, Dec. 2009.

[79] D. R. Smith, S. Schultz, P. Markoš, and C. M. Soukoulis, "Determination of effective permittivity and permeability of metamaterials from reflection and transmission coefficients," *Phys. Rev. B, Condens. Matter*, vol. 65, no. 19, Apr. 2002, Art. no. 195104.

[80] D. R. Smith, D. C. Vier, T. Koschny, and C. M. Soukoulis, "Electromagnetic parameter retrieval from inhomogeneous metamaterials," *Phys. Rev. E, Stat. Phys. Plasmas Fluids Relat. Interdiscip. Top.*, vol. 71, no. 3, Mar. 2005, Art. no. 036617.

[81] X. Chen, T. M. Grzegorczyk, B.-I. Wu, J. Pacheco, and J. A. Kong, "Robust method to retrieve the constitutive effective parameters of metamaterials," *Phys. Rev. E, Stat. Phys. Plasmas Fluids Relat. Interdiscip. Top.*, vol. 70, no. 1, Jul. 2004, Art. no. 016608.

[82] Z. Szabó, G.-H. Park, R. Hedge, and E.-P. Li, "A unique extraction of metamaterial parameters based on Kramers–Kronig relationship," *IEEE Trans. Microw. Theory Techn.*, vol. 58, no. 10, pp. 2646–2653, Oct. 2010.

[83] A. K. Ramrakhyani, S. Mirabbasi, and M. Chiao, "Design and optimization of resonance-based efficient wireless power delivery systems for biomedical implants," *IEEE Trans. Biomed. Circuits Syst.*, vol. 5, no. 1, pp. 48–63, Feb. 2011.

[84] F. Tahar, R. Saad, A. Barakat, and R. K. Pokharel, "1.06 FoM and compact wireless power transfer system using rectangular defected ground structure resonators," *IEEE Microw. Wireless Compon. Lett.*, vol. 27, no. 11, pp. 1025–1027, Nov. 2017.

[85] D. R. Smith, D. Schurig, J. J. Mock, P. Kolinko, and P. Rye, "Partial focusing of radiation by a slab of indefinite media," *Appl. Phys. Lett.*, vol. 84, no. 13, pp. 2244–2246, Mar. 2004.

[86] A. P. Sample, B. H. Waters, S. T. Wisdom, and J. R. Smith, "Enabling seamless wireless power delivery in dynamic environments," *Proc. IEEE*, vol. 101, no. 6, pp. 1343–1358, Jun. 2013.

[87] S. Y. Hui, "Planar wireless charging technology for portable electronic products and qi," *Proc. IEEE*, vol. 101, no. 6, pp. 1290–1301, Jun. 2013.

[88] J. Deng, W. Li, T. D. Nguyen, S. Li, and C. C. Mi, "Compact and efficient bipolar coupler for wireless power chargers: Design and analysis," *IEEE Trans. Power Electron.*, vol. 30, no. 11, pp. 6130–6140, Nov. 2015.

[89] K. A. Cota, P. A. Gray, M. Pathmanathan, and P. W. Lehn, "An approach for selecting compensation capacitances in resonance-based EV wireless power transfer systems with switched capacitors," *IEEE Trans. Transport. Electrific.*, vol. 5, no. 4, pp. 1004–1014, Dec. 2019.

[90] Y. Liu, U. K. Madawala, R. Mai, and Z. He, "Zero-phase-angle controlled bidirectional wireless EV charging systems for large coil misalignments," *IEEE Trans. Power Electron.*, vol. 35, no. 5, pp. 5343–5353, May 2020.

[91] A. Ibrahim and M. Kiani, "A figure-of-merit for design and optimization of inductive power transmission links for millimeter-sized biomedical implants," *IEEE Trans. Biomed. Circuits Syst.*, vol. 10, no. 6, pp. 1100–1111, Dec. 2016.

[92] K. Zhang, C. Liu, Z. H. Jiang, Y. Zhang, X. Liu, H. Guo, and X. Yang, "Near-field wireless power transfer to deep-tissue implants for biomedical applications," *IEEE Trans. Antennas Propag.*, vol. 68, no. 2, pp. 1098–1106, Feb. 2020.

[93] R. Narayanamoorthi, "Modeling of capacitive resonant wireless power and data transfer to deep biomedical implants," *IEEE Trans. Compon., Packag., Manuf. Technol.*, vol. 9, no. 7, pp. 1253–1263, Jul. 2019.

[94] N. Zheludev and Y. Kivshar, "From metamaterials to metadevices," *Nature Mater.*, vol. 11, pp. 917–924, 2012.

[95] M. Song, K. Baryshnikova, A. Markvart, P. Belov, E. Nenasheva, C. Simovski, and P. Kapitanova, "Smart table based on a metasurface for wireless power transfer," *Phys. Rev. A, Gen. Phys.*, vol. 11, no. 5, May 2019, Art. no. 195104.

[96] B.-I. Popa, L. Zigoneanu, and S. A. Cummer, "Tunable active acoustic metamaterials," *Phys. Rev. B, Condens. Matter*, vol. 88, no. 2, Jul. 2013, Art. no. 024303.

[97] F. Casadei, T. Delpero, A. Bergamini, P. Ermanni, and M. Ruzzene, "Piezoelectric resonator arrays for tunable acoustic waveguides and metamaterials," *J. Appl. Phys.*, vol. 112, no. 6, Sep. 2012, Art. no. 064902.

[98] A. L. A. K. Ranaweera, T. S. Pham, V. Ngo, and J.-W. Lee, "Active metamaterial designs for dyanamically controllable wireless power transfer applications," in *Proc. URSI Asia–Pacific Radio Sci. Conf. (URSI AP-RASC)*, Seoul, South Korea, Aug. 2016, pp. 850–853.

[99] A. L. A. K. Ranaweera, T. S. Pham, H. N. Bui, V. Ngo, and J.-W. Lee, "An active metasurface for field-localizing wireless power transfer using dynamically reconfigurable cavities," *Sci. Rep.*, vol. 9, no. 1, pp. 1–12, Aug. 2019.

[100] *IEEE Standard for Safety Levels With Respect to Human Exposure to Radio Frequency Electromagnetic Fields*, IEEE C95.1, 3kHz to 300 GHz IEEE Standards Coordinating Committee, 1999.

[101] T. Shaw and D. Mitra, "Metasurface-based radiative near-field wireless power transfer system for implantable medical devices," *IET Microw., Antennas Propag.*, vol. 13, no. 12, pp. 1974–1982, Oct. 2019.

[102] M. Wang, H. Liu, P. Zhang, X. Zhang, H. Yang, G. Zhou, and L. Li, "Broadband implantable antenna for wireless power transfer in cardiac pacemaker applications," *IEEE J. Electromagn., RF Microw. Med. Biol.*, early access, Jun. 1, 2020, doi: 10.1109/JERM.2020.2999205.

[103] L. Li, H. Liu, H. Zhang, and W. Xue, "Efficient wireless power transfer system integrating with metasurface for biological applications," *IEEE Trans. Ind. Electron.*, vol. 65, no. 4, pp. 3230–3239, Apr. 2018.

WOOSOL LEE (Graduate Student Member, IEEE) received the B.S. degree in statistical information analysis and military art and science from the Korea Military Academy, Seoul, South Korea, in 2011, and the M.S. degree in network centric warfare (computer engineering) from Ajou University, Suwon, South Korea, in 2016. He is currently pursuing the Ph.D. degree in electrical and computer engineering with the University of Florida, Gainesville, FL, USA.

His current research interests include metamaterials for RF/microwave applications, wireless power transfer, RF energy harvesting, RF passive components designing, and low-loss conductors for high-frequency applications.
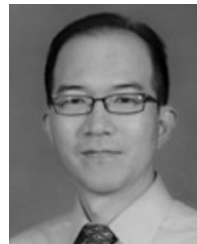
YONG-KYU YOON (Member, IEEE) received the Ph.D. degree in electrical and computer engineering from the Georgia Institute of Technology, Atlanta, GA, USA, in 2004.

He held a postdoctoral researcher position with the Georgia Institute of Technology, from 2004 to 2006. He was an Assistant Professor with the Department of Electrical Engineering, The State University of New York, Buffalo, NY, USA, from 2006 to 2010. He joined the University of Florida, Gainesville, FL, USA, as an Associate Professor, in 2010, where he is currently a Professor and a Graduate Coordinator with the Department of Electrical and Computer Engineering. He spent his sabbatical leave at Seoul National University, from July 2017 to December 2017. He has authored over 200 peer-reviewed publications. His current research interests include microelectromechanical systems, nanofabrication, and energy storage devices; metamaterials for RF/microwave applications; micromachined millimeter wave/terahertz antennas and waveguides; wireless power transfer and telemetry systems; lab-on-a-chip devices; and ferroelectric materials for memory and tunable RF devices. He was a recipient of the NSF Early Career Development Award, in 2008, and the SUNY Young Investigator Award, in 2009.

• • • •